Microstructural Design of Fiber Composites

Tsu-Wei Chou

Book DOI: http://dx.doi.org/10.1017/CBO9780511600272

Online ISBN: 9780511600272

Hardback ISBN: 9780521354820

Paperback ISBN: 9780521019651

Chapter

5 - Hybrid composites pp. 231-284

Chapter DOI: http://dx.doi.org/10.1017/CBO9780511600272.006

Cambridge University Press

5 Hybrid composites

5.1 Introduction

The term 'hybrid composites' is used to describe composites containing more than one type of fiber materials. Hybrid composites are attractive structural materials for the following reasons. First, they provide designers with the new freedom of tailoring composites and achieving properties that cannot be realized in binary systems containing one type of fiber dispersed in a matrix. Second, a more cost-effective utilization of expensive fibers such as carbon and boron can be obtained by replacing them partially with less expensive fibers such as glass and aramid. Third, hybrid composites provide the potential of achieving a balanced pursuit of stiffness, strength and ductility, as well as bending and membrane related mechanical properties. Hybrid composites have also demonstrated weight savings, reduced notch sensitivity, improved fracture toughness, longer fatigue life and excellent impact resistance (Chou and Kelly 1980a). Some of the pioneering studies on this topic can be found in the work of Wells and Hancox (1971), Hayashi (1972), Kalnin (1972), Hancox and Wells (1973), Bunsell and Harris (1974), Harris and Bunsell (1975), Walton and Majumdar (1975), Aveston and Sillwood (1976), Bunsell (1976), Harris and Bradley (1976), Zweben (1977), Arrington and Harris (1978), Badar and Manders (1978, 1981a,b), Marom, Fischer, Tuler and Wagner (1978), Rybicki and Kanninen (1978), Summerscales and Short (1978), Aveston and Kelly (1980), Wagner and Marom (1982), Fukuda (1983a–c), and Harlow (1983).

Depending upon the arrangements of fibers and pre-preg layers, hybrids can be categorized into the following types. In the first type the different fiber materials are intimately mixed together and infiltrated with a matrix simultaneously. The hybrid in this case is described as *intermingled* (Aveston and Kelly 1980) or *intraply* (Chamis and Lark 1978) (Fig. 5.1a). The second type of hybrid is made by bonding together separate laminae each containing just one type of fiber in a matrix, and is known as *interlaminated* (Aveston and Kelly 1980) or *interply* (Chamis and Lark 1978) (Fig. 5.1b). The third category of hybrids consists of fabric reinforcements where each fabric contains more than one type of fiber and it

can be termed as *interwoven* (Chou and Kelly 1980a) (Fig. 5.1c). Hybrid composites consisting of resin composite plies, metal composite plies and metal foils also have been explained. When a laminated hybrid is composed of plies of different matrices it needs to be fabricated by a consolidation procedure that is compatible with all matrix materials.

Optimization of composite properties can usually be achieved through a suitable combination of fiber types. Reinforcements for hybrids include boron, carbon, glass and aramid fibers. Limited applications of ceramic and metallic filaments have been explored (Renton 1978). Intermediate modulus epoxies, thermoplastics and polyimides are the common polymeric matrices for hybrid composites. Current applications of hybrid composites can be found in aircraft fuselage, wing and tail structures, helicopter rotor blades and automobile parts as well as in an array of sports equipment, ranging from sailboats and racing cars to bicycle frames and hockey sticks.

The fundamental questions pertinent to the study of hybrid composites are (a) how is the load shared among the constituent

Fig. 5.1. Types of hybrid composites: (a) intermingled; (b) interlaminated; and (c) interwoven.

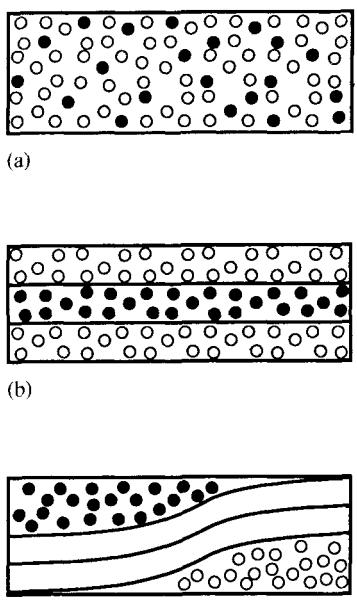

fibers? (b) are there synergistic effects among the different types of fibers? and (c) will certain combinations of fiber types and microstructure designs produce an overall desirable structural performance? In order to gain a basic understanding of these problems, the various aspects of the mechanical behavior of hybrids are examined. To simplify the consideration of deformation, the following discussions are primarily restricted to unidirectional composites and their laminates. Woven hybrid composites are examined in Chapter 6.

5.2 Stress concentrations

The load redistribution in unidirectional continuous fiber hybrid composite laminae due to fiber breakages is examined in this section. Stress concentration factors are obtained for both intermingled and interlaminated hybrids. The solution techniques are demonstrated for both static and dynamic responses. The terminologies of low modulus (LM) and high modulus (HM) are used to distinguish the two kinds of fibers in the model lamina. For hybrid composites such as glass/carbon and Kevlar/carbon combinations, LM and HM fibers correspond to HE (high elongation) and LE (low elongation) fibers, respectively. The fiber ductility or elongation to break does not enter into the present analysis in an explicit manner. The shear-lag technique demonstrated in Chapters 3 and 4 is again adopted in the following.

5.2.1 *Static case*

Consider a unidirectional lamina composed of HM and LM fibers in alternating positions. Each pair of neighboring HM and LM fibers is designated as the group m. Asterisks (*) are used to denote quantities related to LM fibers.

Fukuda and Chou (1983) have examined the three types of combinations of fiber discontinuity depicted in Fig. 5.2. Let n_1 and n_2 be the number of broken HM and LM fibers, respectively. Thus, in Fig. 5.2, (a) $n_1 = n$, $n_2 = 0$; (b) $n_1 = n$, $n_2 = n - 1$; and (c) $n_1 = n_2 = n$. The counting of broken fibers starts at $m = 0$ and ends at $m = n - 1$.

The axial loads of the mth pair of fibers are denoted by $p_m(x)$ and $p_m^*(x)$; the displacements are $u_m(x)$ and $u_m^*(x)$, and $x = 0$ denotes the plane of fiber fracture. Based upon the assumptions of shear-lag analysis (Hedgepeth 1961; Ji, Hsiao and Chou 1981), the force

equilibrium equations of the mth HM and LM fibers are, respectively.

$$Ed\frac{d^2u_m}{dx^2}+\frac{G}{h}(u_m^*+u_{m-1}^*-2u_m)=0$$
$$E^*d^*\frac{d^2u_m^*}{dx^2}+\frac{G}{h}(u_{m+1}+u_m-2u_m^*)=0 \tag{5.1}$$

Here, E and G denote the fiber extensional modulus and the shear modulus of the matrix, respectively. The lamina is assumed to be of unit thickness; d and h denote, respectively, fiber width and spacing.

Under the assumption of linear elastic deformation, the force–displacement relations become

$$p_m=Ed\frac{du_m}{dx},\qquad p_m^*=E^*d^*\frac{du_m^*}{dx} \tag{5.2}$$

Fig. 5.2. Arrays of discontinuous fibers: (a) $n_1=n$, $n_2=0$; (b) $n_1=n$, $n_2=n-1$; (c) $n_1=n_2=n$, n_1 and n_2 are, respectively, the number of discontinuous HM and LM fibers. (After Fukuda and Chou 1983.)

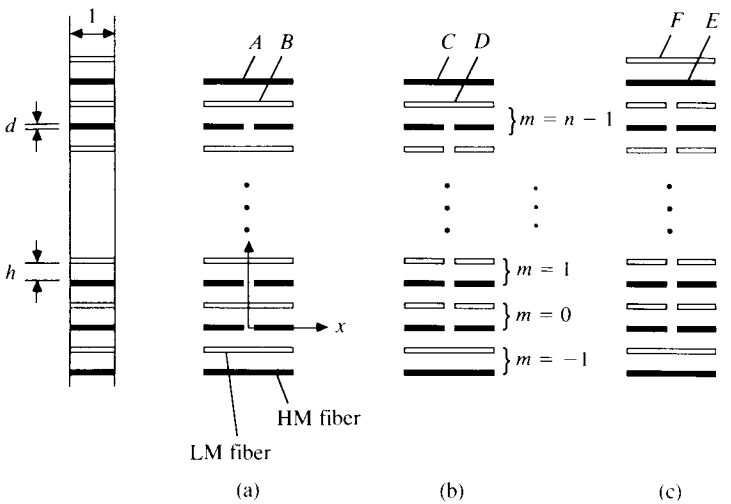

The boundary conditions are

$$
\begin{aligned}
&p_m(\infty) = p \\
&p_m^*(\infty) = \frac{E^* d^*}{Ed} p \\
&p_m(0) = 0, \quad p_m^*(0) = 0 \qquad \text{for broken fibers} \\
&u_m(0) = 0, \quad u_m^*(0) = 0 \qquad \text{for unbroken fibers}
\end{aligned}
\tag{5.3}
$$

To simplify Eqs. (5.1)–(5.3), the following dimensionless parameters are introduced:

$$
\begin{aligned}
&P_m = \frac{p_m}{p} && P_m^* = \frac{p_m^*}{p} \\
&U_m = \frac{u_m}{p}\sqrt{\left(\frac{EdG}{h}\right)} && U_m^* = \frac{u_m^*}{p}\sqrt{\left(\frac{EdG}{h}\right)} \\
&\xi = \sqrt{\left(\frac{G}{Edh}\right)}x && R = E^* d^*/Ed
\end{aligned}
\tag{5.4}
$$

Thus, Eqs. (5.1) and (5.2) become

$$
\frac{\mathrm{d}^2 U_m}{\mathrm{d}\xi^2} + U_m^* + U_{m-1}^* - 2U_m = 0
\tag{5.5}
$$

$$
R\frac{\mathrm{d}^2 U_m^*}{\mathrm{d}\xi^2} + U_{m+1} + U_m - 2U_m^* = 0
$$

$$
P_m = \frac{\mathrm{d}U_m}{\mathrm{d}\xi}
\tag{5.6}
$$

$$
P_m^* = R\frac{\mathrm{d}U_m^*}{\mathrm{d}\xi}
$$

By adopting the concept of influence functions proposed by Hedgepeth (1961), the dimensionless displacements are expressed as

$$
\begin{aligned}
U_m(\xi) &= \xi + \sum_{k=-\infty}^{\infty} V_{m-k}(\xi)U_k(0) + \sum_{k=-\infty}^{\infty} W_{m-k}(\xi)U_k^*(0) \\
U_m^*(\xi) &= \xi + \sum_{k=-\infty}^{\infty} V_{m-k}^*(\xi)U_k(0) + \sum_{k=-\infty}^{\infty} W_{m-k}^*(\xi)U_k^*(0)
\end{aligned}
\tag{5.7}
$$

where V, V^*, W and W^* are the influence functions. Then, from Eqs. (5.5), the following two sets of equations in terms of the influence functions are obtained:

(I)

$$\frac{d^2V_m}{d\xi^2} + V_m^* + V_{m-1}^* - 2V_m = 0$$
$$R\frac{d^2V_m^*}{d\xi^2} + V_{m+1} + V_m - 2V_m^* = 0 \tag{5.8}$$

with the boundary conditions of

$$V_m(0) = 1 \quad (m = 0) \qquad V_m(0) = 0 \quad (m \neq 0)$$
$$V_m^*(0) = 0 \tag{5.9}$$
$$\frac{dV_m(\infty)}{d\xi} = 0 \qquad \frac{dV_m^*(\infty)}{d\xi} = 0$$

(II)

$$\frac{d^2W_m}{d\xi^2} + W_m^* + W_{m-1}^* - 2W_m = 0$$
$$R\frac{d^2W_m^*}{d\xi^2} + W_{m+1} + W_m - 2W_m^* = 0 \tag{5.10}$$

with the boundary condition of

$$W_m(0) = 0$$
$$W_m^*(0) = 1 \quad (m = 0) \qquad W_m^*(0) = 0 \quad (m \neq 0) \tag{5.11}$$
$$\frac{dW_m(\infty)}{d\xi} = 0 \qquad \frac{dW_m^*(\infty)}{d\xi} = 0$$

Since Eqs. (5.8) and (5.10) are identical in form, only the solution procedure of Eqs. (5.8) is given below. For solving Eqs. (5.8), the following Fourier series expressions are introduced

$$\bar{V} = \sum_{m=-\infty}^{\infty} V_m e^{-im\theta} \qquad \bar{V}^* = \sum_{m=-\infty}^{\infty} V_m^* e^{-im\theta} \tag{5.12}$$

or, inversely,

$$V_m = \frac{1}{2\pi}\int_{-\pi}^{\pi} \bar{V} e^{im\theta}\, d\theta \qquad V_m^* = \frac{1}{2\pi}\int_{-\pi}^{\pi} \bar{V}^* e^{im\theta}\, d\theta \tag{5.13}$$

Then, multiplying Eqs. (5.8) by $e^{-im\theta}$ and summing over all m gives

$$\frac{d^2\bar{V}}{d\xi^2} - 2\bar{V} + A\bar{V}^* = 0$$
$$R\frac{d^2\bar{V}^*}{d\xi^2} - 2\bar{V}^* + B\bar{V} = 0 \tag{5.14}$$

where

$$A = 1 + e^{-i\theta} \quad B = 1 + e^{i\theta} \tag{5.15}$$

Also, from Eqs. (5.9),

$$\bar{V}(0, \theta) = 1 \qquad \bar{V}^*(0, \theta) = 0$$
$$\frac{d\bar{V}(\infty, \theta)}{d\xi} = 0 \qquad \frac{d\bar{V}^*(\infty, \theta)}{d\xi} = 0 \tag{5.16}$$

The solutions of Eqs. (5.14) under the boundary conditions of Eqs. (5.16) are

$$\bar{V} = C_1 e^{-\lambda_1\xi} + C_2 e^{-\lambda_2\xi}$$
$$\bar{V}^* = C_3 e^{-\lambda_1\xi} + C_4 e^{-\lambda_2\xi} \tag{5.17}$$

where

$$\lambda_1 = \sqrt{[a + \sqrt{(a^2 - b)}]} \qquad \lambda_2 = \sqrt{[a - \sqrt{(a^2 - b)}]}$$
$$a = 1 + \frac{1}{R} \qquad b = \frac{1}{R}(1 - \cos\theta)$$
$$C_1 = \frac{2 - \lambda_2^2}{\lambda_1^2 - \lambda_2^2} \qquad C_2 = -\frac{2 - \lambda_1^2}{\lambda_1^2 - \lambda_2^2} \tag{5.18}$$
$$C_3 = -\frac{(2 - \lambda_1^2)(2 - \lambda_2^2)}{A(\lambda_1^2 - \lambda_2^2)} \qquad C_4 = -C_3$$

Substituting Eqs. (5.17) into Eqs. (5.13) and considering a, b, λ_1, λ_2, C_1, C_2 and C_3A as even functions with respect to θ, the following results are obtained for the influence functions:

$$V_m = \frac{1}{\pi}\int_0^\pi (C_1 e^{-\lambda_1\xi} + C_2 e^{-\lambda_2\xi})\cos(m\theta)\, d\theta$$
$$V_m^* = \frac{1}{\pi}\int_0^\pi C_3 A(e^{-\lambda_1\xi} - e^{-\lambda_2\xi})\frac{\cos(m\theta) + \cos(m+1)\theta}{2(1 + \cos\theta)}\, d\theta \tag{5.19}$$

Differentiating Eqs. (5.19) and substituting the result for $\xi = 0$ into Eqs. (5.7) and the third condition of Eqs. (5.3), the values of $U_k(0)$ $(0 \le k \le n_1 - 1)$ and $U_k^*(0)$ $(0 \le k \le n_2 - 1)$ can be obtained.

The dimensionless axial loads, P_m and P_m^* are calculated by substituting Eqs. (5.7) into Eqs. (5.6). The stress concentration factor of the mth group of fibers is defined as $P_m(0)/P_m(\infty)$ or $P_m^*(0)/P_m^*(\infty)$.

$$\begin{aligned} P_m(0)/P_m(\infty) &= 1 + \sum_{k=0}^{n_1-1} \frac{dV_{m-k}(0)}{d\xi} U_k(0) \\ &\quad + \sum_{k=0}^{n_2-1} \frac{dW_{m-k}(0)}{d\xi} U_k^*(0) \\ P_m^*(0)/P_m^*(\infty) &= 1 + \sum_{k=0}^{n_1-1} \frac{dV_{m-k}^*(0)}{d\xi} U_k(0) \\ &\quad + \sum_{k=0}^{n_2-1} \frac{dW_{m-k}^*(0)}{d\xi} U_k^*(0) \end{aligned} \tag{5.20}$$

For an HM or an LM fiber adjacent to a discontinuous fiber, the stress concentration factor can be calculated by substituting the corresponding value of m into Eqs. (5.20). For instance, the stress concentration factors for fibers B and A of Fig. 5.2 are, respectively, $P_{n_1-1}^*(0)/P_{n_1-1}^*(\infty)$ and $P_{n_1}(0)/P_{n_1}(\infty)$.

Fukuda and Chou (1981, 1983) have evaluated Eqs. (5.20) and the results are presented for (a) comparisons with the solutions of Hedgepeth (1961) for non-hybrid composites, and (b) hybrid composites. First, for a non-hybrid composite, there is only one type of fiber in the lamina and $R = 1$. Two limiting cases are given below.

(A) $n_1 = 1$ and $n_2 = 0$

Consider, for instance, Fig. 5.2(a). The fiber immediately adjacent to the broken fiber is the one designated as an LM fiber in the $m = 0$ pair. Therefore, the stress concentration factor is

$$P_o^*(0)/P_o^*(\infty) = 1 + \frac{dV_o^*}{d\xi} U_o(0) = \frac{4}{3} \tag{5.21}$$

This result coincides with that of Hedgepeth (1961), as expected. The same conclusion can be reached by considering the case of $n_1 = 0$ and $n_2 = 1$ in Fig. 5.2(a).

(B) $n_1 = n_2 = 1$

The stress concentration factor is given by

$$P_1(0)/P_1(\infty) = 1 + \frac{dV_1(0)}{d\xi} U_o(0) + \frac{dW_1(0)}{d\xi} U_o^*(0)$$

$$= \left(\frac{4}{3}\right)\left(\frac{6}{5}\right) \tag{5.22}$$

Next, for the unidirectional hybrid lamina ($R \neq 1$), Eqs. (5.20) have been solved by numerical integrations using a trapezoidal rule. The results are shown in Figs. 5.3–5.5.

The limiting case of the fracture of one HM fiber ($n_1 = 1$, $n_2 = 0$) is demonstrated in Fig. 5.3. The fibers adjacent to the broken HM fiber of particular interest are the LM fiber of $m = 0$ and the HM fiber of $m = 1$. The stress concentration factors of these two fibers (K_{LM}, K_{HM}) are plotted in Fig. 5.3 as functions of the stiffness ratio $R = E^*d^*/Ed$. For $R = 1$ (i.e. non-hybrid case), $K_{LM} = 1.33$ is obtained from Eq. (5.21). The limit of $R \to 0$, on the other hand, indicates that the extensional rigidity of the LM fiber is infinitesimal. Then Fig. 5.3 again becomes a model with only one type of fiber. The fiber nearest to the broken fiber in this case is the HM fiber of $m = 1$ and therefore $K_{HM} \to \frac{4}{3}$ at the limit $R \to 0$.

Figure 5.3 also indicates that the stress concentration factor of the

Fig. 5.3. Stress concentration factor vs. stiffness ratio $R = E^*d^*/Ed$ = extensional stiffness of LM fiber/extensional stiffness of HM fiber. (After Fukuda and Chou 1981.)

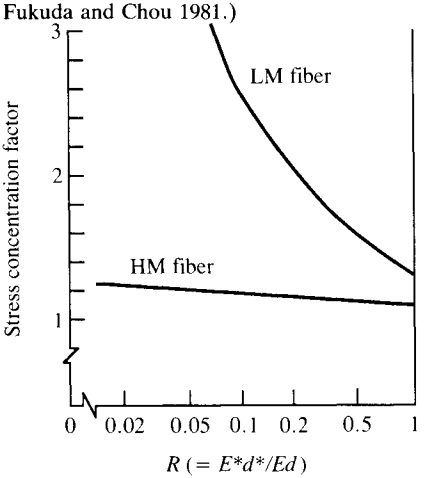

HM fiber in the hybrid lamina is lower than $\frac{4}{3}$ because of the presence of the LM fiber between the discontinuous and continuous HM fibers. For example, at $R = 0.5$, $K_{LM} = 1.67$ and $K_{HM} = 1.11$.

Figure 5.4 depicts the relations between stress concentration factors and the total number of broken fibers, $n_1 + n_2$, for the case of $R = 1$. The letters A–F correspond to fibers A–F in Fig. 5.2. Curves D and E show the stress concentration factors of the fibers immediately adjacent to the broken fibers. Curves C and F give the results for the second nearest fibers to the broken fibers. The cases of A and B in Fig. 5.2 give stress concentration factors insensitive to the number of broken fibers.

Figure 5.5 shows the stress concentration factors for $R = \frac{1}{3}$ which approximately corresponds to carbon/glass hybrid composites. The stress concentration factor of the HM fiber nearest to the discontinuous fibers, i.e. fiber C or E in Figs. 5.2(b) and (c), respectively, is smaller than that of fiber D (Fig. 5.2b) for a fixed number of broken fibers. This means that, as far as the HM fibers are concerned, the stress concentration is reduced in a hybrid composite. Thus, it is possible for the high modulus fibers in a hybrid

Fig. 5.4. Stress concentration factors vs. total number of broken fibers for $R = 1$. (After Fukuda and Chou 1983.)

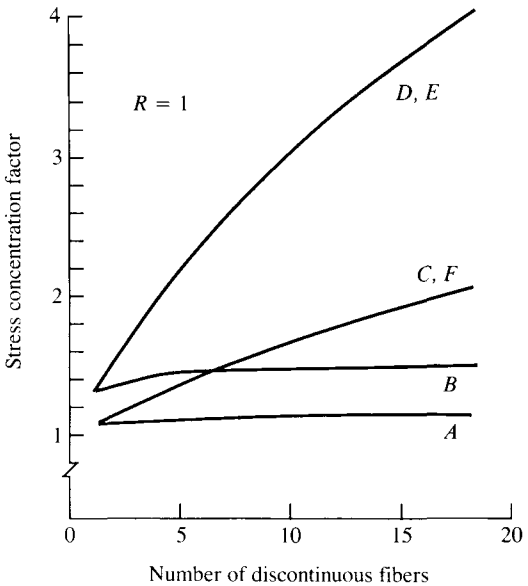

composite to sustain higher loads than in the all-high modulus fiber composite, and a 'hybrid effect' could be realized.

The stress concentration factors of the LM fibers are shown by curves *D* and *F* in Fig. 5.5. A comparison of curves *D* of Figs. 5.4 and 5.5 indicates that the stress concentration on the LM fiber increases as *R* is reduced. This implies that the LM fibers are more susceptible to fracture in a hybrid composite than in a non-hybrid composite.

When the number of fibers in the composite model is high, the solution procedure of the governing equations becomes very complex. Fukunaga, Chou and Fukuda (1984) have evaluated the stress concentration factors using an eigenvector expansion method. Tables 5.1 and 5.2 show the numerical results of their analysis based upon a glass/carbon intermingled hybrid composite ($R = \frac{1}{3}$). The solid and open circles represent HM and LM fibers, respectively.

Fig. 5.5. Stress concentration factors vs. total number of broken fibers for a hybrid composite of $R = \frac{1}{3}$. (After Fukuda and Chou 1983.)

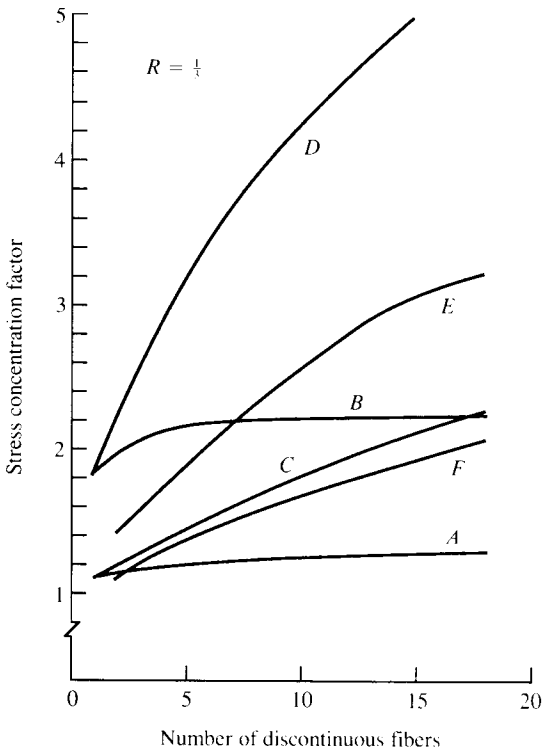

Table 5.1 gives the stress concentration factors for various V_{HM} values, where $K_{ij,k}$, for instance, is the stress concentration factor of the kth fiber due to the breakage of the ith and jth fibers for various fiber relative volume fractions. The fiber arrangements given in Table 5.1 are repeated to generate the composite, but the position

Table 5.1. *Stress concentration factors (SCF) for various V_{HM} values. After Fukunaga, Chou and Fukuda* (1989)

	V_{HM}			
	1.0	0.75	0.5	0.25
	●●●●	●●●○	●○●○	○●○○
SCF	1 2 3 4	1 2 3 4	1 2 3 4	1 2 3 4
$K_{1,2}$	1.333	1.356	1.777	1.141
$K_{1,3}$	1.067	1.077	1.121	1.036
$K_{1,4}$	1.029	1.041	1.060	1.017
$K_{2,1}$	1.333	1.347	1.131	1.829
$K_{2,3}$	1.333	1.347	1.131	1.829
$K_{2,4}$	1.067	1.102	1.030	1.208
$K_{3,1}$	1.067	1.077	1.121	1.036
$K_{3,2}$	1.333	1.356	1.777	1.141
$K_{3,4}$	1.333	1.727	1.777	1.311
$K_{4,1}$	1.029	1.007	1.010	1.017
$K_{4,2}$	1.067	1.018	1.030	1.036
$K_{4,3}$	1.333	1.128	1.131	1.318
$K_{12,3}$	1.600	1.654	1.412	2.144
$K_{12,4}$	1.143	1.221	1.135	1.304
$K_{13,4}$	1.419	1.832	1.952	1.340
$K_{13,2}$	1.802	1.772	2.767	1.291
$K_{14,2}$	1.412	1.378	1.817	1.180
$K_{14,3}$	1.412	1.210	1.261	1.359
$K_{23,1}$	1.600	1.654	1.412	2.144
$K_{23,4}$	1.600	2.275	2.038	1.913
$K_{24,1}$	1.419	1.362	1.146	1.886
$K_{24,3}$	1.802	1.494	1.270	2.252
$K_{34,1}$	1.143	1.109	1.172	1.077
$K_{34,2}$	1.600	1.478	2.038	1.258
$K_{123,4}$	1.829	2.776	2.510	2.175
$K_{234,1}$	1.829	1.768	1.522	2.382
$K_{341,2}$	2.022	1.914	3.105	1.418
$K_{412,3}$	2.022	1.822	1.569	2.612

of the fractured fiber (or fibers) is not repeated. In the numerical calculations 80 fibers are used in each composite model.

Table 5.2 presents the effect of fiber bundle size on stress concentration for the relative fiber volume fraction of $V_{HM} = 50\%$. Two (case 2), three (case 3) or four (case 4) fibers of the same type can be placed adjacent to one another besides the alternating arrangement of one HM and one LM fiber (case 1). It is evident that the stress concentration factor is sensitive to the microscopic fiber arrangements. Knowledge of the stress concentration factors in various hybrid fiber arrays is essential to the evaluation of hybrid composite strength.

5.2.2 *Dynamic case*

The dynamic stress concentration in hybrid composites due to fiber breakage has been examined by Ji, Hsiao and Chou (1981). Figure 5.6 shows an interlaminated hybrid composite for the analytical model; it is composed of a layer of HM fiber and a layer of LM fiber embedded in a common matrix. The fibers are aligned along the x axis, and h_1 and h_2 denote the fiber spacings. A fiber in each array is numbered by an integer n $(-\infty < n < \infty)$. The displacement field of a fiber as a function of location and time is denoted by $u_n(x, t)$ for an HM fiber, and by $u_n^*(x, t)$ for an LM fiber. Similarly, the axial forces in the fibers are denoted by $p_n(x, t)$ and $p_n^*(x, t)$. Ji and colleagues have analyzed the dynamic stress

Table 5.2. *Stress concentration factors for various bundle sizes. After Fukunaga, Chou and Fukuda* (1989)

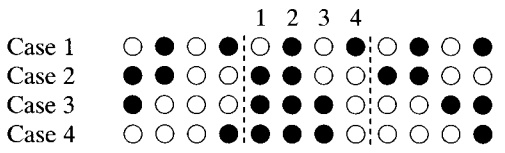

Fiber location	1	2	3	4
Case 1	1.777	×	1.777	1.121
Case 2	1.376	×	1.762	1.175
Case 3	1.354	×	1.354	1.113
	1.082	1.366	×	1.763
Case 4	1.343	×	1.351	1.112
	1.079	1.365	×	1.764

concentration factor of the fiber $n = 1$ or -1 in the HM fiber array when the fiber $n = 0$ suddenly breaks.

The fundamental equations governing the deformation of the HM and LM fibers are approximated by

$$\begin{aligned} EA\frac{\partial^2 u_n}{\partial x^2} + \frac{Gh_1}{h_2}(u_{n+1} - 2u_n + u_{n-1}) + \frac{Gh_2}{h_1}(u_n^* - u_n) \\ = m\frac{\partial^2 u_n}{\partial t^2} \\ E^*A^*\frac{\partial^2 u_n^*}{\partial x^2} + \frac{Gh_1}{h_2}(u_{n+1}^* - 2u_n^* + u_{n-1}^*) + \frac{Gh_2}{h_1}(u_n - u_n^*) \\ = m^*\frac{\partial^2 u_n^*}{\partial t^2} \end{aligned} \tag{5.23}$$

for all n ($= -\infty, \ldots, -1, 0, 1, \ldots, \infty$). In Eqs. (5.23), m and m^* are the fiber masses per unit length, E^* and E are the fiber Young's moduli, A^* and A denote fiber cross-sectional areas, and G is the matrix shear modulus.

The boundary conditions are

$$\begin{aligned} &p_o(0, t) = 0 \\ &u_n(0, t) = 0 \quad (n \neq 0) \qquad p_n(\pm\infty, t) = p \quad (\text{all } n) \\ &u_n^*(0, t) = 0 \quad (\text{all } n) \qquad p_n^*(\pm\infty, t) = \frac{E^*A^*}{EA}p \quad (\text{all } n) \end{aligned} \tag{5.24}$$

Fig. 5.6. A model of interlaminated hybrid composite. (After Ji, Hsiao and Chou 1981.)

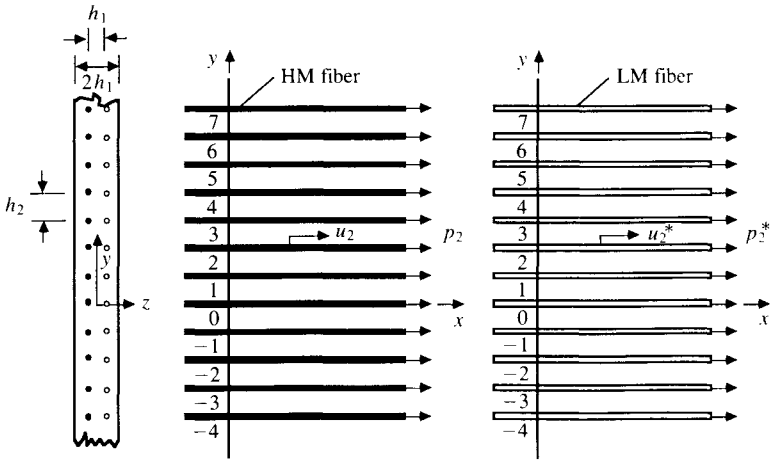

The initial conditions are

$$p_n(x, 0) = p \qquad \frac{\partial u_n}{\partial t}(x, 0) = 0$$
$$p_n^*(x, 0) = \frac{E^*A^*}{EA} p \qquad \frac{\partial u_n^*}{\partial t}(x, 0) = 0 \tag{5.25}$$

for all n.

The forces and displacements of the fibers are related by

$$p_n = EA \frac{\partial u_n}{\partial t} \tag{5.26}$$

By introducing the following dimensionless parameters,

$$P_n = \frac{p_n}{p} \qquad P_n^* = \frac{p_n^*}{p}$$
$$U_n = \frac{u_n}{p} \sqrt{\left(\frac{EAGh_1}{h_2}\right)} \qquad U_n^* = \frac{u_n^*}{p} \sqrt{\left(\frac{EAGh_1}{h_2}\right)}$$
$$\xi = \sqrt{\left(\frac{Gh_1}{EAh_2}\right)} x \qquad \tau = \sqrt{\left(\frac{Gh_1}{mh_2}\right)} t \tag{5.27}$$
$$R = \frac{E^*A^*}{EA} \qquad M = \frac{m^*}{m} \qquad D = \frac{h_2^2}{h_1^2}$$

Eqs. (5.23) can be rewritten as

$$\frac{\partial^2 U_n}{\partial \xi^2} + U_{n+1} - 2U_n + U_{n-1} + D(U_n^* - U_n) = \frac{\partial^2 U_n}{\partial \tau^2}$$
$$R \frac{\partial^2 U_n^*}{\partial \xi^2} + U_{n+1}^* - 2U_n^* + U_{n-1}^* + D(U_n - U_n^*) = \frac{\partial^2 U_n^*}{\partial \tau^2} \tag{5.28}$$

Also, Eqs. (5.24) become

$$P_o(0, \tau) = 0$$
$$U_n(0, \tau) = 0 \quad (n \neq 0), \qquad P_n(\pm\infty, \tau) = 1 \quad (\text{all } n) \tag{5.29}$$
$$U_n^*(0, \tau) = 0 \quad (\text{all } n), \qquad P_n^*(\pm\infty, \tau) = R \quad (\text{all } n)$$

and Eqs. (5.25) can be written in terms of displacements only as

$$U_n(\xi, 0) = \xi \qquad \frac{\partial U_n}{\partial \tau}(\xi, 0) = 0$$
$$U_n^*(\xi, 0) = \xi \qquad \frac{\partial U_n^*}{\partial \tau}(\xi, 0) = 0 \tag{5.30}$$

Equations (5.28)–(5.30) can be solved following the approach of Hedgepeth. Three essential steps are involved: the Laplace transform in time, the use of the technique of influence function, and the Fourier series representation of the unknown functions. Ji and colleagues have evaluated the dynamic stress concentration factor of the HM fibers immediately adjacent to the broken fiber. The most severe stress concentration factor $K_1(0, \tau)$ occurs at $\xi = 0$. It is interesting to note that the solution of $K_1(0, \tau)$ is composed of two parts which are related to the HM and LM fibers, respectively. Figures 5.7–5.9 depict the variation of the stress concentration factor $K_1(0, \tau)$ with the dimensionless time τ for $m^*/m = 1$, 2 and 6, respectively. The two components of the solution are denoted by K_1' and K_1''. Also in these figures, $E^*A^*/EA = h_2/h_1 = 1$. Figure 5.7 is for the case of non-hybrid composites and the solution of Hedgepeth for a unidirectional lamina is also shown. The summation of K_1' and

Fig. 5.7. The variation of stress concentration factor K_1 with dimensionless time τ for $m^*/m = E^*A^*/EA = h_2/h_1 = 1$. K_1' and K_1'' are the two components of K_1. (After Ji, Hsiao and Chou 1981.)

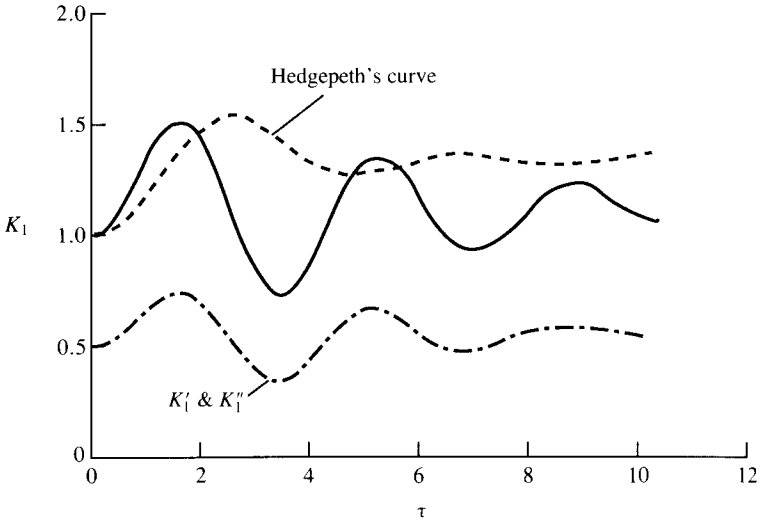

K_1'' gives the total stress concentration factor. As the difference in mass density of the HM and LM fibers increases, the locations of the peak values of K_1' and K_1'' are out of phase. As a result, the maximum value of $K_1' + K_1''$ is reduced (Figs. 5.8 and 5.9).

The analysis of Ji and colleagues concludes that the time variations of the stress concentration factors related to the two component fiber materials are always out of phase in a hybrid composite with fibers of different mass densities. The parent HM fiber composite always provides the upper bound for the stress concentration of the hybrid, since this is the case where there is no difference in phase and magnitude of the K_1' and K_1'' values. Furthermore, the magnitudes of the K_1' and K_1'' are determined by the extensional stiffnesses of the component fibers.

5.3 Tensile stress–strain behavior

An idealized stress–strain curve of a hybrid composite containing both high elongation (HE) and low elongation (LE) fibers is depicted in Fig. 5.10 (Aveston and Kelly 1980). For hybrids with good bonding between the component phases, the stress–strain curve is given by *OABC*. The important features of this curve include the elastic behavior indicated by *OA*, the first cracking

Fig. 5.8. The variation of stress concentration factor K_1 with dimensionless time τ for $m^*/m = 2$, and $E^*A^*/EA = h_2/h_1 = 1$. K_1' and K_1'' are the two components of K_1. (After Ji, Hsiao and Chou 1981.)

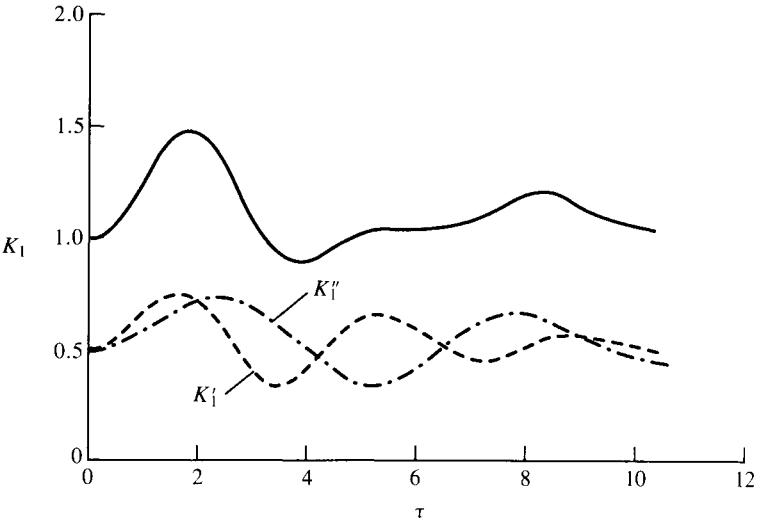

Fig. 5.9. The variation of stress concentration factor K_1 with dimensionless time τ for $m^*/m = 6$, and $E^*A^*/EA = h_2/h_1 = 1$. K_1' and K_1'' are the two components of K_1. (After Ji, Hsiao and Chou 1981.)

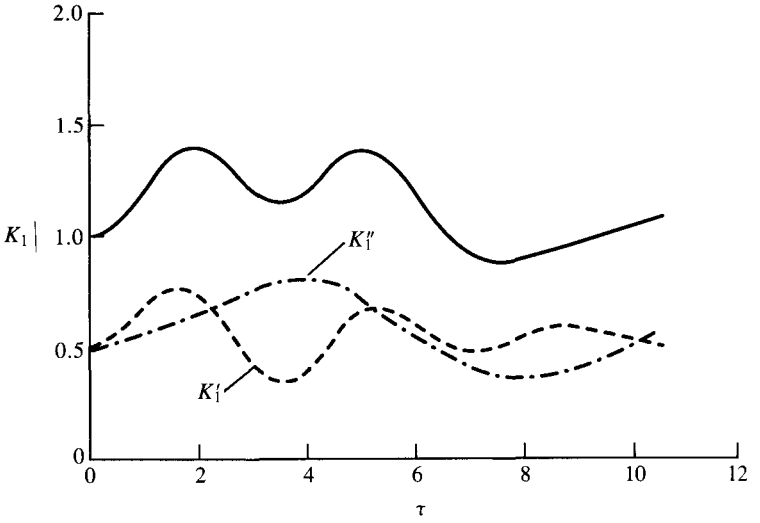

Fig. 5.10. A typical stress–strain curve of hybrid composites. (After Aveston and Kelly 1980.)

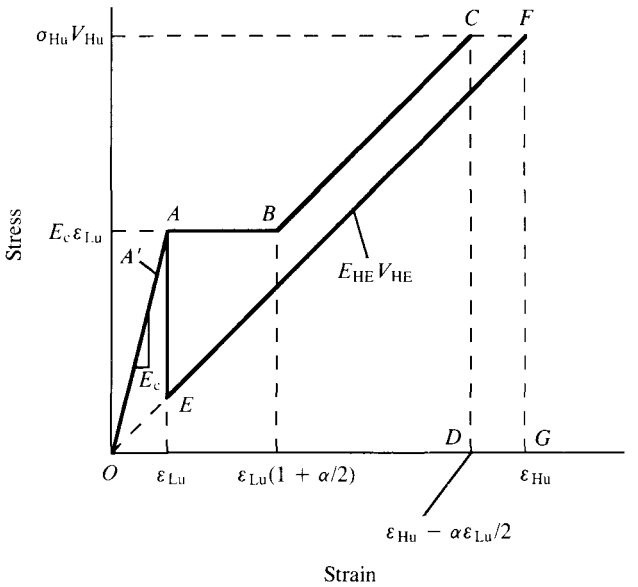

strain ε_{Lu}, the relatively flat portion of the curve AB, the subsequent rise of the curve at a smaller slope (BC) and the final failure strain of the hybrid given by the point D. The subscripts H and L are used to denote parameters related to high and low elongation fibers, respectively. The various features of the stress–strain curve are discussed in the following.

5.3.1 *Elastic behavior*

Theoretical predictions of the elastic moduli of multi-phase short-fiber composites have been performed by Chou, Nomura and Taya (1980) using a self-consistent approach, Nomura and Chou (1984) based upon a bound approach, and Taya and Chou (1984) employing a combination of Eshelby's (1957) equivalent inclusion method and Mori and Tanaka's (1973) back stress analysis.

For unidirectional hybrid composites composed of continuous fibers, Chamis and Sinclair (1979) have examined the elastic properties based upon composite micromechanics approach, linear laminate theory, and finite element analysis. It has been concluded that these methods predict approximately the same elastic properties. The through-the-thickness properties predicted by the micromechanics equations are in good agreement with the finite element results.

For simplicity, the results from the micromechanics approach are introduced below. The analytical model is an intermingled hybrid composite composed of two components, termed *primary composite* and *secondary composite* by Chamis and Sinclair (Fig. 5.11). Since these two components are interchangeable, they can be

Fig. 5.11. An intermingled hybrid composite lamina composed of primary (HM) and secondary (LM) phases.

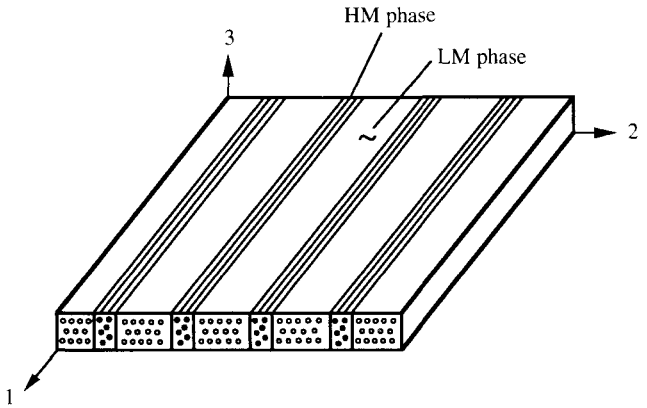

considered the high modulus (HM) and low modulus (LM) components. In the following, the subscripts 1, 2 and 3 denote, respectively, the directions along the fiber, transverse to the fiber and through the thickness in an intermingled hybrid lamina.

The effective longitudinal Young's modulus is approximated by the iso-strain assumption along the 1-direction:

$$E_{11} = E_{11}^{HM} + (E_{11}^{LM} - E_{11}^{HM})V_{LM} \tag{5.31}$$

Here, E_{11}^{HM} and E_{11}^{LM} denote the longitudinal Young's moduli of the HM and LM composites, respectively. V_{LM} is the volume fraction of the LM composite and $V_{LM} + V_{HM} = 1$. Both E_{11}^{HM} and E_{11}^{LM} can be expressed in terms of the properties of the fiber and matrix as given in Eqs. (2.7).

The transverse Young's modulus is obtained by assuming that the HM and LM components are connected in series in the 2-direction

$$E_{22} = E_{22}^{HM} \Big/ \left[1 + \left(\frac{E_{22}^{HM}}{E_{22}^{LM}} - 1\right)V_{LM}\right] \tag{5.32}$$

Here, E_{22}^{HM} and E_{22}^{LM} are the transverse Young's moduli of the HM and LM composites, respectively. E_{22}^{HM} and E_{22}^{LM} can also be expressed in terms of fiber and matrix elastic properties as well as the fiber volume fraction of each component phase (Eqs. (2.7)).

The effective Young's modulus in the through-the-thickness direction has been modeled by Chamis and Sinclair assuming that the component phases are in parallel in the 3-direction. Thus,

$$E_{33} = E_{33}^{HM} + (E_{33}^{LM} - E_{33}^{HM})V_{LM} \tag{5.33}$$

Here, E_{33}^{HM} and E_{33}^{LM} are the transverse Young's moduli of the unidirectional composites composed of HM and LM fibers, respectively. Since the unidirectional all-HM or all-LM fiber composite is assumed to be transversely isotropic the expression of E_{33} $(=E_{22})$ of Eqs. (2.7) can be used to relate $E_{33}^{HM}(E_{33}^{LM})$ to the constituent material properties. However, it should be noted that for a yarn-by-yarn unidirectional intermingled hybrid lamina, $E_{22} \neq E_{33}$ and thus the composite is not transversely isotropic.

The in-plane shear modulus G_{12} is obtained by an iso-stress approximation

$$G_{12} = G_{12}^{HM} \Big/ \left[1 + \left(\frac{G_{12}^{HM}}{G_{12}^{LM}} - 1\right)V_{LM}\right] \tag{5.34}$$

Similarly, the interlaminar shear modulus G_{23} is expressed as

$$G_{23} = G_{23}^{HM} \Big/ \left[1 + \left(\frac{G_{23}^{HM}}{G_{23}^{LM}} - 1\right) V_{LM}\right] \tag{5.35}$$

The interlaminar shear modulus G_{13} is obtained by assuming that the component phases are connected in parallel in the 3-direction. Thus analogous to Eq. (5.31) the following expression can be obtained:

$$G_{13} = G_{13}^{HM} + (G_{13}^{LM} - G_{13}^{HM}) V_{LM} \tag{5.36}$$

in Eqs. (5.34)–(5.36), the shear moduli of the component phases can again be related to the constituent fiber and matrix properties by using Eqs. (2.7).

The Poisson's ratios ν_{12} and ν_{32} are derived by assuming parallel elements in the 1- and 3-directions.

$$\nu_{12} = \nu_{12}^{HM} + (\nu_{12}^{LM} - \nu_{12}^{HM}) V_{LM} \tag{5.37}$$

$$\nu_{32} = \nu_{32}^{HM} + (\nu_{32}^{LM} - \nu_{32}^{HM}) V_{LM} \tag{5.38}$$

For the derivation of ν_{13}, the iso-strain and iso-stress states are assumed in the 1- and 3-directions, respectively. The result is

$$\nu_{13} = \nu_{13}^{HM} + \frac{V_{LM}(\nu_{13}^{LM} - \nu_{13}^{HM})}{(1 - V_{LM})\dfrac{E_{33}^{HM}}{E_{33}^{LM}} + V_{LM}} \tag{5.39}$$

Experimental measurements of the elastic properties of intermingled hybrid composites can be found in the work of Chamis and Sinclair (1979) and Gruber and Chou (1983). The thermal properties of unidirectional intermingled hybrid composites have also been examined by Chamis and Sinclair (1979). It has been recommended that linear laminate theory be used to predict the thermal expansion coefficients.

5.3.2 *First cracking strain*

The linear portion of the stress–strain curve often extends beyond the failure strain of the pure LE fiber composite (point A' in Fig. 5.10) and the first cracking of the LE fibers occurs at the strain ε_{Lu} (point A in Fig. 5.10). This phenomenon is known as a 'hybrid effect'. The treatment of fiber first cracking strain of Aveston and Kelly (1980) is introduced below.

A unidirectional hybrid composite composed of both high and low elongation components can continue to bear the total load after

the first cracking of the low elongation component if the following condition is satisfied:

$$V_{HE} \geq \frac{\sigma_{Lu}}{\sigma_{Hu} + \sigma_{Lu} - \sigma'_H} \tag{5.40}$$

Here, σ_u denotes the failure stress, V indicates fiber volume fraction, the subscripts L and H denote the LE and HE components, respectively. Also, σ'_H $(=\varepsilon_{Lu}E_H)$ is the stress of the HE component at the failure strain of the LE component. For both HE and LE components behaving elastically up to ε_{Lu}, the above condition can also be expressed in terms of the failure strain of the high elongation component

$$\varepsilon_{Hu} \geq \varepsilon_{Lu}(1 + \alpha) \tag{5.41}$$

where

$$\alpha = \frac{E_{LE}V_{LE}}{E_{HE}V_{HE}} \tag{5.42}$$

and E denotes the Young's modulus. Obviously the effect of stress redistribution due to fiber breakage is not considered here.

The magnitude of the first cracking strain ε_{Lu} and the extension of the curve between A and B in Fig. 5.10 can be understood using the concept of multiple cracking and constrained failure (Chapter 3). It has been established that the first failure strain is size dependent. The term *size* means essentially the effective diameters of fiber tows and their spacings at a fixed fiber volume content as well as the thickness of lamellae in an interlaminated hybrid.

When an interlaminated hybrid composite is deformed beyond the first cracking strain, parallel cracks will appear in the low elongation phase with the crack planes normal to the loading axis. The spacing of the cracks depends on the bonding (i.e. elastic or frictional) between the component plies, after the initial cracking. If they remain elastically bonded, the crack spacing is determined by the maximum interfacial shear stress at the crack, τ_{max}. On the other hand, if load transfer occurs through frictional bonds between the component phases, the crack spacing is determined by the limiting bond strength τ. In both cases, the formation of a crack through the ply thickness of the low elongation component results in the relaxation of the material in this ply on both sides of the crack. The nearly flat portion of the composite stress–strain curve, i.e. AB in Fig. 5.10, is the consequence of multiple cracking of the low elongation phase and the associated extension of the specimen.

The stress originally carried by the low elongation component on the crack plane has to be shifted to the high elongation phase. The maximum additional stress thrown onto the high elongation phase can be estimated by

$$\Delta\sigma = \frac{\sigma_a}{V_{HE}} - \frac{\sigma_a E_{HE}}{E_c} \tag{5.43}$$

where σ_a is the applied stress and E_c is the Young's modulus of the composite. The first term on the right-hand side of Eq. (5.43) is the stress on the crack plane while the second term gives the stress away from the crack plane in the high elongation component. The additional load carried by the high elongation component induces an extension δl of the specimen ends.

The idea of load transfer between the HE and LE components explains why the strain ε_{Lu}, at which first cracking occurs, depends upon the dispersion of the component phases. When thinner fibers or lamellae are used, the interfacial area per unit volume between the two component phases increases. This also means increased efficiency of load transfer from the HE component bridging the crack back to the LE layers. As a result, the additionally strained length of this component and, hence, the displacement of the specimen ends, δl, are decreased. The product of δl and $E_c\varepsilon_{Lu}$ gives the upper limit of the work available from the loading system to form the crack. Assuming a constant surface work of fracture γ, the decrease in δl will reach such a point that ε_{Lu} must increase above the value for the pure LE composite before the required work of fracture can be extracted from the system. In the case of interlaminated hybrids with an elastically bonded interface the cracking strain of the low elongation phase of thickness d can be estimated by (Aveston and Kelly 1980)

$$\varepsilon_{Lu} = \sqrt{\left[\frac{2\gamma_{LE}V_{LE}}{E_c\alpha}\sqrt{\left(\frac{E_c G_{LE}}{E_{HE}E_{LE}}\right)}\frac{1}{\sqrt{(V_{HE})d}}\right]} \tag{5.44}$$

where α is defined in Eq. (5.42). Equation (5.44) predicts that ε_{Lu} varies with the inverse square root of ply thickness. This prediction of the hybrid effect is consistent with the experimental observation of carbon/glass sandwich laminates that the carbon ply failure strain is greater when its absolute thickness is smaller.

The theory of multiple cracking in fiber composites has very broad applicability. Multiple cracking occurs in the brittle phase which could be either the matrix or the fiber phase of an aligned fiber

composite, the low elongation layers of a non-hybrid laminated composite, or the layers reinforced with LE fibers in an interlaminated hybrid composite. Multiple cracking of non-hybrid composites has been examined in Chapter 3. Aveston and Kelly (1980) have summarized the analytical expressions of the minimum crack spacings, the first cracking strain and the maximum interfacial stress for hybrid and non-hybrid composites with both elastic and sliding friction bonds.

The above discussions have provided the answer to the question posed in Section 5.1 concerning synergistic effects in hybrid composites. The answer to the question of load sharing is also positive. The bond between the fiber and matrix in a hybrid ensures that the LE fiber continues to carry part of the applied load and to contribute to the overall stiffness after first cracking (Bunsell and Harris 1974). The load sharing by the LE fiber is evident from the observation of multiple fractures in well bonded interply hybrids and by the bursts of acoustic emission accompanying the repeated load drops on the stress–strain curve. Finally, the rise of curve *BC* in Fig. 5.10 is attributed to the loading of the high elongation fibers. The failure strain of the hybrid composite (point *D*) is lower than that of the high elongation fiber composite (point *G*). This is because the multiple fracture of the LE fibers and partial debonding between the HE and LE fiber reinforced laminae. Consequently, the HE layers in an interlaminated hybrid composite cannot be stretched uniformly along their length to the ultimate strain level. On the other hand, if the debonding is complete at the first fiber cracking strain, ε_{Lu}, the stress–strain curve follows the path *OAEF*. Note that *EF* and *BC* in Fig. 5.10 have the same slope.

5.3.3 *Differential Poisson's effect*

Another factor that needs to be taken into account in the deformation of hybrid composites is the interlaminar stress induced due to differential Poisson's effect (Aveston and Kelly 1980). It is understood that this effect exists in laminated composites with or without fiber hybridization. To demonstrate the magnitude of the Poisson's strain and its effect on longitudinal splitting of laminated composites, a three-layer non-hybrid cross-ply laminate is considered. The central LE (90°) layer in this case is sandwiched between two HE (0°) layers. Thus the conclusions derived from this example are applicable to interlaminated composites in general. The strain induced by the differential Poisson's effect depends only on

the volume fraction of the component phases. However, cracking of the lamina can be minimized by making the LE layers sufficiently thin.

The critical strain for causing longitudinal split due to Poisson's effect can be derived based upon Fig. 3.25. Let the subscripts 1 and 2 denote the longitudinal and transverse fiber directions, respectively, and x–y–z are the reference axes of the cross-ply. Under a simple extension ε_{yy}, the following strains are induced in the 0° and 90° layers, if they are deformed independently:

$$\begin{aligned} \varepsilon_{xx}(0°) &= -\nu_{12}\varepsilon_{yy} \\ \varepsilon_{xx}(90°) &= -\nu_{21}\varepsilon_{yy} \end{aligned} \tag{5.45}$$

For the composite laminate subjected to ε_{yy}, the strain induced in the x direction is ε_{xx}. Referring to Fig. 3.25, the transverse strains induced in the 0° and 90° layers due to the Poisson effect are

$$\begin{aligned} \Delta\varepsilon_{xx}(0°) &= \varepsilon_{xx} - \varepsilon_{xx}(0°) = \varepsilon_{xx} + \nu_{12}\varepsilon_{yy} \\ \Delta\varepsilon_{xx}(90°) &= \varepsilon_{xx} - \varepsilon_{xx}(90°) = \varepsilon_{xx} + \nu_{21}\varepsilon_{yy} \end{aligned} \tag{5.46}$$

Thus

$$\Delta\varepsilon_{xx}(0°) - \Delta\varepsilon_{xx}(90°) = (\nu_{12} - \nu_{21})\varepsilon_{yy} \tag{5.47}$$

The stress σ_{xx} is built up in each layer due to the requirement of compatibility in normal strain in the x direction. These stresses are given approximately by

$$\begin{aligned} \sigma_{xx}(0°) &= \Delta\varepsilon_{xx}(0°)E_{22} \\ \sigma_{xx}(90°) &= \Delta\varepsilon_{xx}(90°)E_{11} \end{aligned} \tag{5.48}$$

The force equilibrium of the laminate in the transverse direction requires

$$\sigma_{xx}(0°)b + \sigma_{xx}(90°)h = \Delta\varepsilon_{xx}(0°)E_{22}b + \Delta\varepsilon_{xx}(90°)E_{11}h = 0 \tag{5.49}$$

From Eqs. (5.47) and (5.49), the transverse strain induced in the 0° layer due to the Poisson's effect is

$$\Delta\varepsilon_{xx}(0°) = \frac{E_{11}h(\nu_{12} - \nu_{21})\varepsilon_{yy}}{(h + b)E_c} \tag{5.50}$$

where $E_c = E_{22}(b/h + b) + E_{11}(h/h + b)$ is the effective Young's modulus along the x direction.

If the 0° and 90° layers in the laminate of Fig. 3.25 are of different materials, then it is necessary to distinguish the elastic constants in Eq. (5.50)

$$\Delta\varepsilon_{xx}(0°) = \frac{E_{11}(90°)h[\nu_{12}(0°) - \nu_{21}(90°)]\varepsilon_{yy}}{bE_{22}(0°) + hE_{11}(90°)} \tag{5.51}$$

5.3.4 *Differential thermal expansion*

Additional strain may be induced in a laminated hybrid composite due to differential thermal expansion of the component phases. The carbon/glass hybrid system is a typical case where the axial thermal expansion coefficient of the glass laminae is much larger than that of the carbon layers. Upon cooling down from the stress-free temperature, compressive stress develops in the carbon layers as a result of the differential thermal expansion. This thermally induced compression can partially account for the hybrid effect often observed in carbon/glass hybrids (Bunsell and Harris 1974). The constrained thermal strain in such a hybrid with high and low elongation fibers can be expressed as (Aveston and Kelly 1980)

$$\varepsilon_{LE}^{T} = \frac{\Delta T E_{HE} V_{HE}}{E_c}(\alpha_{LE} - \alpha_{HE}) \tag{5.52}$$

$$\varepsilon_{HE}^{T} = \frac{\Delta T E_{LE} V_{LE}}{E_c}(\alpha_{HE} - \alpha_{LE}) \tag{5.53}$$

where ΔT = stress-free temperature − service temperature, and α_{LE} and α_{HE} denote the thermal expansion coefficients. The thermal strain components are independent of fiber or lamina dimension. The relation between the cracking strain and the dimension of the low elongation phase is identical under external load and thermal load. Hence, the treatment of multiple cracking can still be applied in this case.

5.4 Strength theories

Discussions on the strength of hybrid composites begin with an introduction on the rule-of-mixtures type of approach which delineates the contributions of the high elongation and low elongation fibers to the load carrying capacity of the hybrid. In this approach, the fibers are assumed to be of uniform strength and the local stress redistributions due to fiber breakage are not taken into

account. This is then followed by the probabilistic strength theories. The synergistic effects between the LE and HE fibers in local stress concentration and fiber strength distributions are modeled to predict the first failure strength and ultimate failure strength of hybrid composites.

5.4.1 *Rule-of-mixtures*

The ultimate tensile strength of a unidirectional hybrid composite can be estimated from the contributions of the component phases at different volume fractions. Consider a binary composite with low elongation fibers. The addition of a small amount of higher elongation fiber decreases the strength of the composite. The ultimate hybrid composite tensile strength, σ_{cu}, is given by (Aveston and Kelly 1980)

$$\sigma_{cu} = \sigma_{Lu} V_{LE} + \varepsilon_{Lu} E_{HE} V_{HE} \tag{5.54}$$

where ε_{Lu} is the failure strain of the LE fiber in the hybrid. The failure of the low elongation fiber leads to the fracture of the hybrid and there is no multiple fracture.

As the content of the high elongation fiber increases, a transition in failure mode occurs when there is sufficient volume of these fibers to carry the load upon the fracture of the low elongation fibers. The fracture mode is multiple fracture of the brittle fibers. The ultimate tensile strength is represented by

$$\sigma_{cu} = \sigma_{Hu} V_{HE} \tag{5.55}$$

The volume fraction of HE fibers should exceed the lower limit, given by Eq. (5.40), to bear the total load at the first cracking strain. Aveston and Kelly (1980) applied Eqs. (5.54) and (5.55) to analyze the experimental data of Kalnin (1972), who studied the failure stress of interlaminated carbon/glass/epoxy hybrids. Figure 5.12 shows the variation of hybrid composite ultimate tensile strength with the relative glass fiber content. The stress is calculated by dividing the load by the cross-sectional area of the fiber and, thus, the contribution of the epoxy matrix is neglected. Aveston and Kelly suggested that for this particular experimental system the fracture of carbon fibers did not produce a large stress concentration leading to the weakening of the glass fibers.

5.4.2 *Probabilistic initial failure strength*

It has been shown in Section 5.3.2 that the phenomena of initial failures of unidirectional hybrid composites and cross-ply

laminates share the same basic physical principle. In unidirectional hybrid composites consisting of LE and HE fibers, the failure strain of the LE fibers under tension is often greater than that in the all LE fiber composite. On the other hand, in the non-hybrid $[\pm\theta°/90°]_s$ $(0° < \theta < 90°)$ laminates the failure strength (strain) of the 90° (LE) layer under tension is greater for smaller thickness of the inner 90° layers. It is also known that the failure strength (strain) of the inner 90° layer depends on the material properties of the outer $\pm\theta°$ layers. Thus, in composites which consist of laminae with two different types of material properties such as hybrid composites and $[\pm\theta°/90°]_s$ non-hybrid laminates, the failure strength (strain) of the LE layers is not an intrinsic material property and it depends on the HE material properties and the geometric arrangement of the layers.

Fukunaga, Chou and Fukuda (1984) and Fukunaga *et al.* (1984a&b) have examined the initial failure strength of both hybrid and non-hybrid composites based upon a statistical approach. The hybrid composite under consideration is a sandwiched structure composed of unidirectional glass fiber and carbon fiber laminae (Fig. 5.13a). The non-hybrid composite is a carbon composite with the $[\pm\theta°/90°]_s$ configuration (Fig. 5.13b). Both composites can be depicted by the HE and LE representations of Fig. 5.13(c) where M_{HE} and M_{LE} denote, respectively, the number of HE and LE

Fig. 5.12. Tensile strength of aligned carbon/glass/epoxy hybrids vs. relative fiber content. (After Aveston and Kelly 1980.)

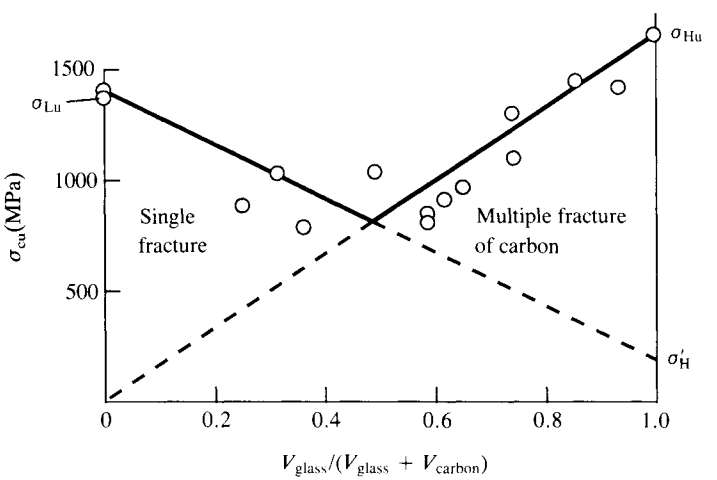

layers. Thus, the total number of layers in the hybrid composite, $M = M_{HE} + M_{LE}$.

Fukunaga and colleagues modeled the composite as a chain of short laminates in series as shown in Fig. 3.17. Each laminate has the length δ equivalent to the ineffective length, and the specimen length $l = N\delta$. In order to obtain the first ply failure strength of the whole laminated composite, the following two-parameter cumulative Weibull distribution functions of failure strain for the LE and HE short layers are assumed

$$F_{LE}(\varepsilon) = 1 - \exp[-(\varepsilon/\varepsilon^*_{LE})^{\beta_{LE}}]$$
$$F_{HE}(\varepsilon) = 1 - \exp[-(\varepsilon/\varepsilon^*_{HE})^{\beta_{HE}}] \tag{5.56}$$

Here ε^* and β denote the scale and shape parameters, respectively. Then, the cumulative distribution function $H_c(\varepsilon)$ for the first ply failure strain of the composite can be obtained from the weakest link model

$$H_c(\varepsilon) = 1 - [1 - G_c(\varepsilon)]^N \tag{5.57}$$

where $G_c(\varepsilon)$ is the cumulative distribution function for the first ply failure strain of the short laminate and it is given by

$$G_c(\varepsilon) = 1 - [1 - F_{LE}(\varepsilon)]^{M_{LE}}[1 - F_{HE}(\varepsilon)]^{M_{HE}} \tag{5.58}$$

Fig. 5.13. (a) Carbon/glass hybrid laminate. (b) $[\pm\theta°/90°]_s$ non-hybrid laminate. (c) Model for analysis. (After Fukunaga *et al.* 1984c.)

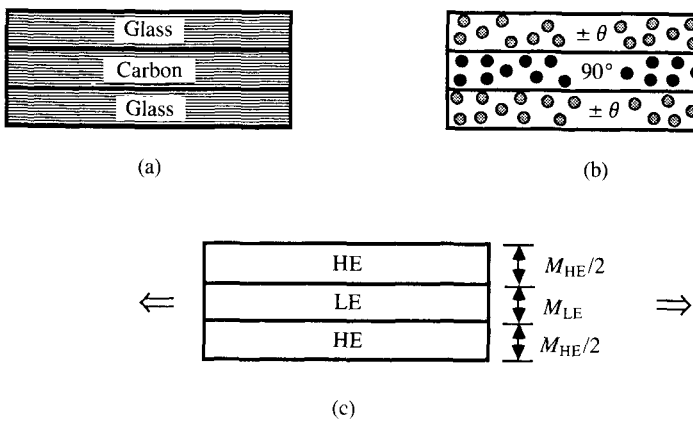

Substitution of Eq. (5.58) into Eq. (5.57) yields

$$H_c(\varepsilon) = 1 - \exp[-NM_{LE}(\varepsilon/\varepsilon^*_{LE})^{\beta_{LE}} - NM_{HE}(\varepsilon/\varepsilon^*_{HE})^{\beta_{HE}}] \tag{5.59}$$

It should be noted that Eq. (5.59) is concerned with the first ply failure strain of the composite laminate not the LE phase of the composite. This is because, from a probabilistic viewpoint, the failure of the LE layer does not always precede that of the HE layers. Similar to Eq. (5.59) the cumulative distribution function $H_{LE}(\varepsilon)$ for the first ply failure strain of the all LE fiber composite (of the same size as the hybrid composite) is given by

$$H_{LE}(\varepsilon) = 1 - \exp[-NM(\varepsilon/\varepsilon^*_{LE})^{\beta_{LE}}] \tag{5.60}$$

Fukunaga and colleagues have compared the failure strains for the HE/LE/HE laminate and the pure LE laminate for the failure strains at 50% failure probability. From Eqs. (5.59) and (5.60)

$$\begin{aligned} &\frac{M_{LE}}{M}\left(\frac{\varepsilon_c}{\varepsilon^*_{LE}}\right)^{\beta_{LE}} + \frac{M_{HE}}{M}\left(\frac{\varepsilon_c}{\varepsilon^*_{HE}}\right)^{\beta_{HE}} = \frac{\ln 2}{NM} \\ &\left(\frac{\varepsilon_{LE}}{\varepsilon^*_{LE}}\right)^{\beta_{LE}} = \frac{\ln 2}{NM} \end{aligned} \tag{5.61}$$

where ε_c and ε_{LE} denote, respectively, the median failure strains of the hybrid and LE composite. In order to obtain an explicit relation between the ratio of median failure strains, $\varepsilon_c/\varepsilon_{LE}$, and the relative volume fraction of the LE material, M_{LE}/M, the case of $\beta_{LE} = \beta_{HE} = \beta$ is considered. Then, Eqs. (5.61) become

$$\frac{\varepsilon_c}{\varepsilon_{LE}} = \left(\frac{M_{LE} + M_{HE}/(\varepsilon^*)^{\beta}}{M}\right)^{-1/\beta} \tag{5.62}$$

where $\varepsilon^* = \varepsilon^*_{HE}/\varepsilon^*_{LE}$. The ratio $\varepsilon_c/\varepsilon_{LE}$ in Eq. (5.62) is independent of the size of the composite. By assuming linear stress–strain relations for the HE and LE layers, the first ply failure strength ratio σ_c/σ_{LE} is readily obtained

$$\frac{\sigma_c}{\sigma_{LE}} = \frac{E_c}{E_{LE}}\left(\frac{M_{LE} + M_{HE}/(\varepsilon^*)^{\beta}}{M}\right)^{-1/\beta} \tag{5.63}$$

where E denotes the Young's modulus in the loading direction, $E_c = (M_{LE}E_{LE} + M_{HE}E_{HE})/M$.

Numerical calculations of Eqs. (5.62) and (5.63) have been performed for carbon/glass/epoxy unidirectional hybrid composites. It is assumed that $\varepsilon^* = 3.0$ and $E_{HE}/E_{LE} = \frac{1}{3}$. Figure 5.14 shows the comparison of Eq. (5.62) with the experimental results of Bader and Manders (1981a&b) for HTS carbon/glass hybrid laminates. The analytical results for $\beta = 10$ seem to show good agreement with experimental results. Figure 5.15 indicates the variation of initial composite failure strength with the relative volume fraction of LE and HE layers. Points A and D in Fig. 5.15 represent the strengths of glass and carbon composites, respectively. Line $BD(\sigma_c/\sigma_{LE} = E_c/E_{LE})$ indicates the stress in the hybrid at which failure of the carbon layer takes place. Line $AE(\sigma_c/\sigma_{LE} = M_{HE}/(M_{LE} + M_{HE}))$ represents the stress in the hybrid assuming that the LE layer carries no load. As the shape parameter β decreases, the first ply failure strain and strength of the hybrid composite increase relative to those of the all carbon fiber composite. When $\beta \to \infty$, that is for composites without scattering in the failure strains of the LE and HE layers, the first ply failure strain of the hybrid composite is identical to that of the pure LE composite. This relation at $\beta \to \infty$ in Fig. 5.15 is equivalent to the rule-of-mixtures for the initial failure in hybrids.

Fig. 5.14. Comparisons of the analytical predictions of Fukunaga *et al.* (1984c) and the experimental results of Bader and Manders (1981a&b) for HTS carbon/E-glass hybrid laminates. (After Fukunaga *et al.* 1984c.)

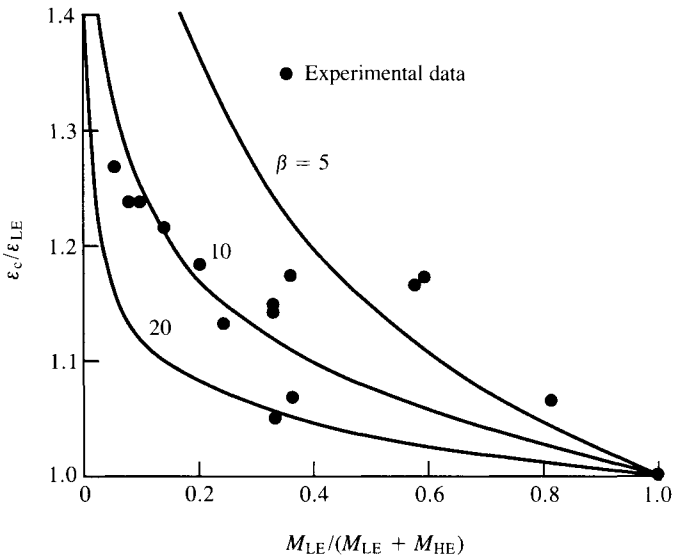

The trend of variation of $\varepsilon_c/\varepsilon_{LE}$ with the relative 90° layer volume fraction for $[\pm\theta°/90°]_s$ laminates is similar to that given in Fig. 5.14. For a given value of shape parameter, $\varepsilon_c/\varepsilon_{LE}$ decreases with the increase in the angle θ.

In summary, the probabilistic strength analysis of Fukunaga, Chou and Fukuda (1984) and Fukunaga *et al.* (1984a) for the initial failure in hybrid and non-hybrid composites has demonstrated a volumetric relation. It has been shown that the initial failure strain or strength is greater in composites composed of low elongation and high elongation materials than in the all low elongation fiber composite. This is the result of a 'size effect'; that is the failure probability is lower in the composite with the smaller size of the low elongation material.

5.4.3 *Probabilistic ultimate failure strength*

In this section three analytic approaches are presented for predicting the ultimate tensile strength of hybrid composites. All these methods consider the variability in fiber strength and the stress redistribution at fiber fracture. First, the analytical model of Zweben (1977) assumes that the LE and HE fibers are arranged in alternating positions in a unidirectional lamina. The fracture of an

Fig. 5.15. Composite initial failure strength σ_c (normalized by σ_{LE}) in glass/carbon/glass laminates. $\beta_{LE} = \beta_{HE} = \beta$, $\varepsilon^*_{HE} = \varepsilon^*_{LE} = 3.0$ and $E_{HE}/E_{LE} = \frac{1}{3}$. (After Fukunaga *et al.* 1984c.)

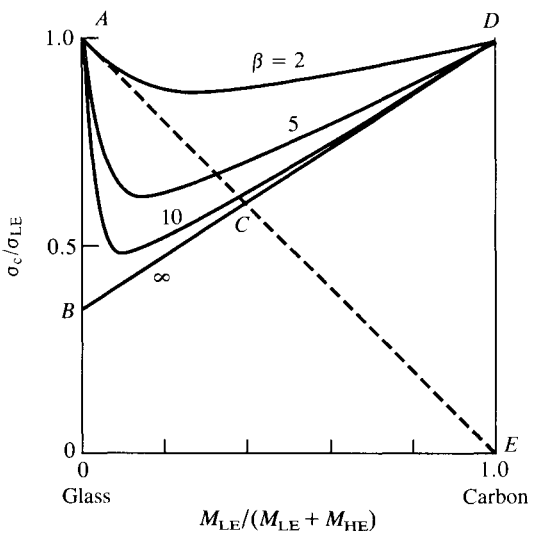

LE fiber induces, in the vicinity of the fiber fracture, a local stress (strain) concentration. The HE fibers will break at the points of stress (strain) concentration. Zweben hypothesizes that the strain level at which the first overstressed HE fiber is expected to break is a lower bound on the ultimate strain of the hybrid composite.

Next, in order to obtain a more realistic view of the multiple fracture of the LE fibers in a hybrid composite, Fukuda and Chou (1982a&b) adopted a Monte-Carlo simulation of the ultimate failure of a unidirectional hybrid composite. The method demonstrates the diffused nature of fracture of the LE fibers. The constraint on the propagation of the LE fiber fractures due to the presence of HE fibers as well as the stress–strain relation of the hybrid composite as influenced by multiple fiber fractures has been demonstrated.

Thirdly, Fukunaga, Chou and Fukuda (1989) have adopted a more rigorous approach by applying the methods of Harlow and Phoenix (1978a&b). The effects on the ultimate strength of hybrid laminates due to the scatter of laminar strengths, relative fiber volume fractions, composite size and laminate stacking sequence have been identified.

The analytical model of Zweben is composed of a single layer of fibers of axial length l with the same arrangement as that shown in Fig. 3.17. High elongation (low modulus) fibers and low elongation (high modulus) fibers are arranged in alternating positions. The total number of fibers in the composite is M, of which $M/2$ are LE, and $M/2$ are HE fibers. The term 'fibers', according Zweben, represents both single fibers and yarns.

It is assumed that the fibers support all of the applied load and the fibers break under load in a random fashion throughout the composite. Attention is focussed on what happens in the vicinity of the breaks in the LE fibers. The strain of the composite is adopted as the independent variable. When an LE fiber breaks at the strain level ε, the two adjacent HE fibers are subjected to a strain concentration of $K_h\varepsilon$, where K_h is the strain concentration factor associated with a single broken LE fiber. Because of the linear elastic deformation assumed in the model, K_h is also the stress concentration factor. Since the model assumes that the fiber axial stress depends only on the axial strain, the stress in these two HE fibers increases from $E_{HE}\varepsilon$ to $K_h E_{HE}\varepsilon$. The axial distance over which the fiber stress is perturbed due to a fiber breakage is known as the ineffective length (Rosen 1964). Zweben denoted the ineffective length associated with a broken LE fiber in the hybrid by δ_h.

Similar to Fig. 3.17, the hybrid composite is composed of a series of links with axial dimension δ_h. The total number of links is $N_h = l/\delta_h$. Failure of the composite results from the propagation of fiber breaks due to local strain concentrations.

The cumulative distribution functions for the failure strains of the LE and HE fibers of length l are assumed in the form of Weibull distributions:

$$F_{LE}(\varepsilon) = 1 - \exp(-pl\varepsilon^q)$$
$$F_{HE}(\varepsilon) = 1 - \exp(-rl\varepsilon^s) \tag{5.64}$$

where p, q, r and s are Weibull parameters. The composite strain at which the fracture of the first overstressed HE fibers occurs in the hybrid is given by

$$\varepsilon_h = [Mlpr\delta_h(K_h^s - 1)]^{-1/(q+s)} \tag{5.65}$$

For a composite reinforced with M fibers of the same type, say the LE fibers, Eq. (5.65) becomes

$$\varepsilon = [2Mlp^2\delta_{LE}(K_{LE}^q - 1)]^{-1/2q} \tag{5.66}$$

Here, K_{LE} and δ_{LE} are, respectively, the strain concentration factor and ineffective length of the LE fiber composite.

From Eqs. (5.65) and (5.66), Zweben has obtained the ratio of the lower bounds of failure strain of a hybrid to that of a LE fiber composite of the same length

$$R = \frac{\varepsilon_h}{\varepsilon} = \frac{[Mlpr\delta_h(K_h^s - 1)]^{-1/(q+s)}}{[2Mlp^2\delta_{LE}(K_{LE}^q - 1)]^{-1/2q}} \tag{5.67}$$

Equation (5.67) indicates that the ratio of the failure strains depends on the Weibull strength parameters p, q, r and s, the specimen length l, the ineffective lengths δ_h and δ_{LE}, and the strain concentration factors K_{LE} and K_{HE}. Zweben has derived approximate expressions of these parameters in terms of the fiber elastic properties and the geometric parameters of fiber arrangements in the composites.

For the convenience of assessing the failure characteristics of hybrid composites, Eq. (5.67) can be simplified by assuming that both LE and HE fibers have the same coefficient of variation in tensile failure strain. It can be shown that for this case $q = s$ and Eq. (5.67) becomes

$$R = \left(\frac{r}{p}\right)^{-1/2q}\left[\frac{\delta_h(K_h^q - 1)}{2\delta_{LE}(K_{LE}^q - 1)}\right]^{-1/2q} \tag{5.68}$$

From Eq. (3.54a) the mean strains of the LE and HE fibers for the gauge-length l are given by

$$\bar{\varepsilon}_{\mathrm{LE}}(l) = (pl)^{-1/q}\Gamma\left(1+\frac{1}{q}\right)$$
$$\bar{\varepsilon}_{\mathrm{HE}}(l) = (rl)^{-1/s}\Gamma\left(1+\frac{1}{s}\right) \tag{5.69}$$

where Γ is a gamma function. Thus, for $q = s$, Eqs. (5.68) and (5.69) yield

$$R = \sqrt{\left(\frac{\bar{\varepsilon}_{\mathrm{HE}}}{\bar{\varepsilon}_{\mathrm{LE}}}\right)}\left[\frac{\delta_{\mathrm{h}}(K_{\mathrm{h}}^{q}-1)}{2\delta_{\mathrm{LE}}(K_{\mathrm{LE}}^{q}-1)}\right]^{-1/2q} \tag{5.70}$$

Equation (5.70) can be further simplified if the fiber coefficient of variation is small (i.e. 5% or less) and thus the shape parameter is large ($q > 25$). For this case $K_{\mathrm{HE}}^{q} - 1 \approx K_{\mathrm{HE}}^{q}$ and $K^{q} - 1 \approx K^{q}$, and Eq. (5.70) is reduced to

$$R = 2^{1/2q}\sqrt{\left(\frac{\bar{\varepsilon}_{\mathrm{HE}}}{\bar{\varepsilon}_{\mathrm{LE}}}\right)}\left(\frac{\delta_{\mathrm{LE}}}{\delta_{\mathrm{h}}}\right)^{1/2q}\sqrt{\left(\frac{K_{\mathrm{LE}}}{K_{\mathrm{h}}}\right)} \tag{5.71}$$

Equation (5.71) indicates that the ratio of the lower bounds of failure strains is sensitive to the mean fiber failure strains and the strain concentration factors and it is less sensitive to the ineffective lengths under the assumption of low fiber coefficient of variations. For the case of an intermingled Kevlar 49/Thornel 300 hybrid composite, Zweben obtained $K_{\mathrm{h}} = 1.462$, $K_{\mathrm{LE}} = 1.293$, $\delta_{\mathrm{h}}/\delta_{\mathrm{LE}} = 1.573/1.531 = 1.03$, and $\bar{\varepsilon}_{\mathrm{HE}}/\bar{\varepsilon}_{\mathrm{LE}} = 1.63$. The fiber strain coefficients of variation for both HE and LE fibers are assumed to be about 6% if the Weibull parameter $q = 20$ is adopted. Using these values, Eq. (5.71) gives $R = 1.22$.

In spite of the simplifying assumption used, Zweben's model, in essence, predicts that the introduction of HE fibers into a LE fiber composite enhances the failure strain of the hybrid composite. This effect is attributed to the ability of HE fibers to redistribute the local stress concentration and act like crack arrestors at the micromechanical level.

Fukuda and Chou (1982a) have examined the strength of hybrid composites using the method of Monte Carlo simulation. Figure 5.16 shows an idealized intermingled hybrid composite sheet of unit thickness. The LE and HE fibers assume alternating positions. For the purpose of numerical calculations, a five-fiber region with three LE fibers and two HE fibers is considered. Following the notations

of the chain-of-links model given in Fig. 3.17, $M = 5$ and $N = 20$ are adopted for Fig. 5.16. Also the extensional rigidity ratios $R(= E^*d^*/Ed)$ are assumed to be unity (for a non-hybrid composite) and $\frac{1}{3}$ (for simulating a glass/carbon composite).

Using a shear-lag analysis, the stress concentration factors are evaluated. The fiber breakage patterns considered by Fukuda and Chou include all the combinations of one-, two-, three- and four-fiber fracture in a transverse plane. A shear-lag analysis is applied to evaluate the stress concentration factors of all the intact links in the layer where fiber breakage has taken place. Results for two kinds of fiber composites are presented below.

In the first case, there is only one type of fiber; its strength follows a normal distribution with an average normalized strength of unity and a standard deviation of 0.1. A typical sequence of link failure is shown in Fig. 5.17(a), where 0 indicates that the link is intact and the other numbers show the sequence of fracture of links. In this model, the link of $i = 14$, $j = 2$ breaks first; the link of $i = 5$, $j = 4$ breaks second; finally the failure occurs at the transverse plane of $i = 14$. In a total of 100 links, six links are broken. One hundred iterations have been performed by Fukuda and Chou and the number of broken links of each iteration is found to be either five or six. Generally speaking, multiple fiber fractures are not extensive in non-hybrid composites.

Fig. 5.16. Model for the Monte Carlo simulation. (After Fukuda and Chou 1982a.)

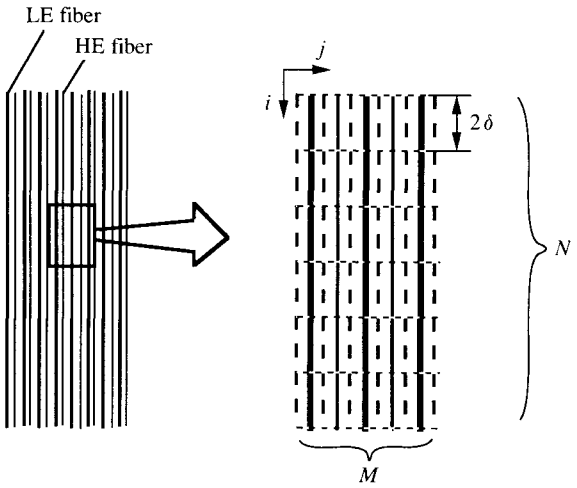

Figure 5.17(b) shows the failure sequence of links in the hybrid composite. It is seen that the LE fibers tend to break at the initial stage of loading and that a total of 16 links are broken for this model to fail at the plane of $i = 10$. A minimum of five and a maximum of 32 link failures are observed during 100 iterations, and the average number of broken links in one iteration is 16.3. The degree of multiple fiber fracture is considerably more extensive in the hybrid composite than the non-hydrid case.

Figure 5.18 shows the examples of stress–strain relations of both non-hybrid and hybrid composites. The stress σ_c and strain ε_c of composites are normalized by the average ultimate stress (σ_{LINK}) and average ultimate strain (ε_{LINK}) of the links of LE fibers. The initial failure strains of the LE fiber composite and the hybrid composite are nearly the same. However, in the hybrid composite, initial multiple failures of the LE fibers are arrested by the HE fibers. As a result, the hybrid composite can withstand more deformation and hence a higher ultimate failure strain. According

Fig. 5.17. Examples of the fiber link failure sequence. (a) Non-hybrid composite. (b) Hybrid composite. (After Fukuda and Chou 1982a.)

0	0	0	0	0	0	0	0	0	0
0	0	0	0	0	0	0	0	0	2
0	0	0	0	0	0	0	0	0	0
0	0	0	0	0	0	0	0	0	0
0	0	0	2	0	0	0	0	0	0
0	0	0	0	0	0	0	0	0	0
0	0	0	0	0	10	0	13	0	14
0	0	0	0	0	0	0	11	0	0
0	0	0	0	0	3	0	4	0	0
0	0	0	0	0	7	16	8	15	1
0	0	0	0	0	0	0	0	0	0
0	0	0	0	0	9	0	0	0	0
0	0	0	0	0	0	0	0	0	0
3	1	4	5	6	0	0	0	0	0
0	0	0	0	0	0	0	0	0	0
0	0	0	0	0	0	0	0	0	0
0	0	0	0	0	0	0	0	0	0
0	0	0	0	0	0	0	0	0	0
0	0	0	0	0	0	0	0	0	0
0	0	0	0	0	12	0	6	0	5
					LE	HE	LE	HE	LE
		(a)					(b)		

to this example, the ultimate strain increases approximately 50% over that of the LE fiber composite.

Although the total number of fibers utilized in this numerical model is extremely small the progressive nature of failure as indicated in the stress–strain curve resembles that of the experimental curves obtained by Bunsell and Harris (1974) of carbon/glass hybrid composites.

The ultimate strength of the hybrid predicted in Fig. 5.18 is lower than those of the LE and HE fiber composites and the ultimate strain of the hybrid is lower than that of the HE fiber composite. This can be understood from the fact that, with the exception of those on the crack plane, the links of the HE fibers are constrained by the surrounding LE links and cannot be deformed to their ultimate strain. As a result, the strength potential of the HE links is not fully realized.

Fukunaga, Chou and Fukuda (1989) have extended the treatment of Harlow and Phoenix (1978a&b) to analyze the ultimate tensile strength of hybrid composites. In their model, the laminate is also treated as a chain of N short segments arranged in series. Each segment has a length δ and the total length of the composite is $l = N\delta$. There are four layers in the laminate. Figure 5.19 shows the stacking sequence of the laminates consisting of LE and HE fiber layers. The strain concentration factors for the various configurations of layer breakage have been evaluated by the eigenvector expansion method (Fukunaga, Chou and Fukuda 1984).

Fig. 5.18. Normalized stress–strain relations of non-hybrid and hybrid composites. (After Fukuda and Chou 1982a.)

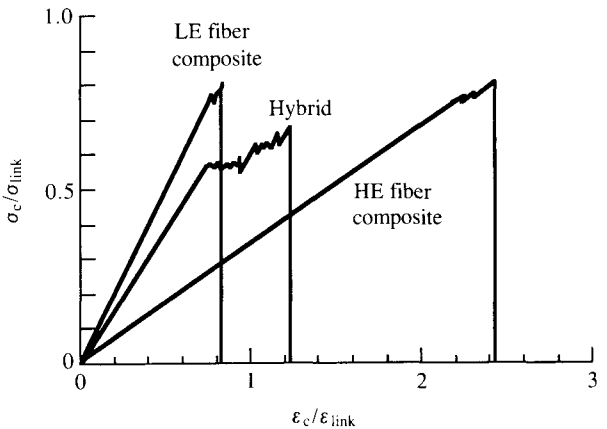

The strength analysis is performed on the basis of the knowledge of the stress redistribution due to layer breakage. It is assumed that each layer follows a two-parameter Weibull probability distribution function and the ultimate failure is defined as the failure of all the layers. The cumulative distribution functions for the ultimate strains of the LE and HE layers are denoted by $F_{LE}(\varepsilon)$ and $F_{HE}(\varepsilon)$, respectively. They are expressed as in Eqs. (5.56). The failure patterns of the four-layered hybrid are shown in Fig. 5.20 where the circles and crosses denote the intact and broken layers, respectively; the possibilities of one, two, three, and four fractured layers are given. According to Fukunaga and colleagues, there are altogether 75 possible failure sequences which can be grouped into eight

Fig. 5.19. Stacking sequences of laminates. (After Fukunaga, Chou and Fukuda 1989.)

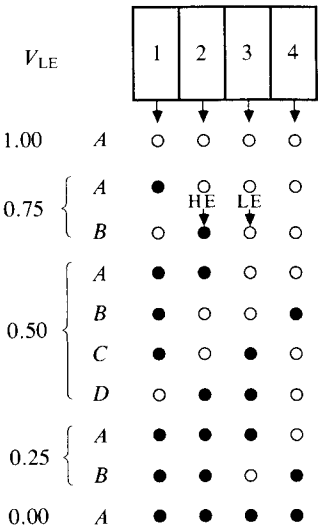

Fig. 5.20. Failure patterns of the four-layered hybrid composite. (After Fukunaga, Chou and Fukuda 1989.)

	b : x o o o	*f* : x x o o	*l* : x x x o	
	c : o x o o	*g* : x o x o	*m* : x x o x	
a : o o o o	*d* : o o x o	*h* : x o o x	*n* : x o x x	*p* : x x x x
: 1 2 3 4	*e* : o o o x	*i* : o x x o	*o* : o x x x	
		j : o x o x		
		k : o o x x		

different types. The number of different failure sequences in each type has been identified. A typical failure sequence in each type and the corresponding failure probability are given in Table 5.3 where $F(x)$ stands for $F_{LE}(\varepsilon)$ for the LE layer and $F_{HE}(\varepsilon)$ for the HE layer, and $K_{ij,k}$ denotes the strain concentration factor of the kth layer due to the fracture of the ith and jth layers.

The cumulative distribution function, $G(\varepsilon)$, in failure strain for a laminate segment of length δ is given by the summation of the failure probabilities of failure sequences no. 1 through no. 75. When $G(\varepsilon)$ is given, the cumulative distribution function with respect to the average stress, $G(\sigma)$ can be obtained from the relation $\sigma = E_c\varepsilon$, where E_c is the effective axial Young's modulus of the hybrid laminate. Finally, the cumulative distribution function, $H(\sigma)$, for the hybrid composite of length $l = N\delta$ is given by the weakest link theory as follows:

$$H(\sigma) = 1 - [1 - G(\sigma)]^N \tag{5.72}$$

Two limiting cases are considered. In the case of non-hybrid composites, $F_{LE}(\varepsilon) = F_{HE}(\varepsilon)$, the above results can be reduced to those of Harlow and Phoenix if the local load sharing (equal load sharing) rule is used for the strain redistribution. Another case deserving attention is the situation of high failure probability, for which the first ply failure may trigger the complete failure of the laminate. The cumulative distribution function for the first ply failure strength of a laminate segment is then given by Eq. (5.58)

Table 5.3. *Failure sequence and failure probability of the four-layered hybrid composite*

Type	Nos.	Failure sequence	Failure probability
I	1–24	*abflp*	$F(x)\{F(K_{1,2}x) - F(x)\}\{F(K_{12,3}x) - F(K_{1,3}x)\}\{F(K_{123,4}x) - F(K_{12,4}x)\}$
II	25–36	*ablp*	$F(x)\{F(K_{1,2}x) - F(x)\}\{F(K_{1,3}x) - F(x)\}\{F(K_{123,4}x) - F(K_{1,4}x)\}$
III	37–48	*abfp*	$F(x)\{F(K_{1,2}x) - F(x)\}\{F(K_{12,3}x) - F(K_{1,3}x)\}\{F(K_{12,4}x) - F(K_{1,4}x)\}$
IV	49–60	*aflp*	$F(x)^2\{F(K_{12,3}x) - F(x)\}\{F(K_{123,4}x) - F(K_{12,4}x)\}$
V	61–4	*abp*	$F(x)\{F(K_{1,2}x) - F(x)\}\{F(K_{1,3}x) - F(x)\}\{F(K_{1,4}x) - F(x)\}$
VI	65–70	*afp*	$F(x)^2\{F(K_{12,3}x) - F(x)\}\{F(K_{12,4}x) - F(x)\}$
VII	71–4	*alp*	$F(x)^3\{F(K_{123,4}x) - F(x)\}$
VII	75	*ap*	$F(x)^4$

with ε replaced by σ. Fukunaga and colleagues have shown that $G(\sigma)$ can be expressed on the Weibull probability paper in the following form:

$$\ln\{-\ln(1-G(\sigma))\} = \beta \ln\frac{\sigma}{\sigma_o} + \beta \ln\frac{M}{M_{LE}+M_{HE}E} + \ln(M_{LE}+M_{HE}E^{\beta}) \tag{5.73}$$

where $M = M_{LE} + M_{HE}$, $E = E_{HE}/E_{LE}$ and σ_o is the scale parameter.

Numerical results of the hybrid ultimate strength have been obtained for $\beta = \beta_{LE} = \beta_{HE}$, $E_{HE}/E_{LE} = \frac{1}{3}$ and $\varepsilon^*_{HE} = \varepsilon^*_{LE} = 3$. Figure 5.21 shows the median strength for $V_{LE} = 0.5$ and four different laminate configurations. It can be seen that the strength of hybrid laminates with LE layers clustering together (cases A and B in Fig. 5.21) is lower than that for the situation where the LE layers are dispersed more evenly among the HE layers. This obviously results from the higher stress concentration factors in cases A and B than in cases C and D.

Figure 5.22 shows the median strength variation with V_{LE} for the case of $N = 100$. The points A (A') and D (D'), respectively, represent the strengths of an all HE fiber composite and an all LE fiber composite. Line BD ($B'D'$) represents the stress in the

Fig. 5.21. Effects of stacking sequences on the median strength. (After Fukunaga, Chou and Fukuda 1989.)

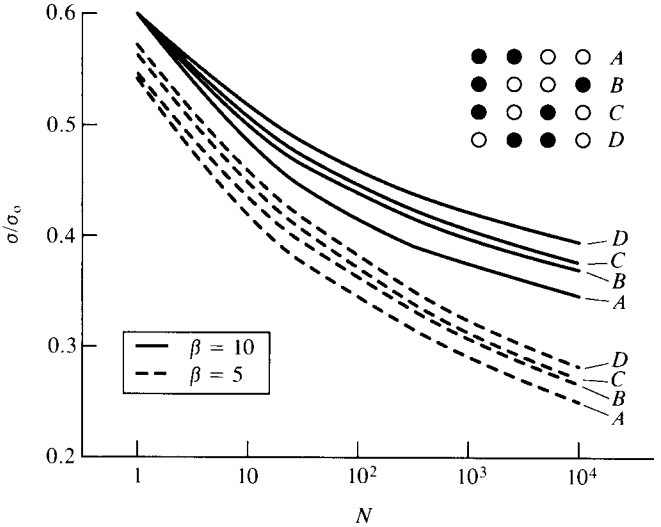

hybrid at which failure of the LE fiber takes place. Line AC ($A'C'$) represents the stress in the hybrid assuming that the LE fibers carry no load. According to the rule-of-mixtures, line AED ($A'E'D'$) marks the ultimate failure strength of the hybrid. Increases in strength above the rule-of-mixtures are known as a hybrid effect. The present results show that the strength of hybrid laminates is lower than that of the all LE and all HE fiber composites. This finding is consistent with the experimental measurements of hybrid laminate strength (Ji 1982). Some other effects on the strength can also be seen from this figure. These are the scatter of the lamina strengths, the LE fiber relative volume fraction and the laminate stacking sequence. The median strength for $\beta = 10$ is greater than that for $\beta = 5$, whereas the hybrid effect is greater for $\beta = 5$ than that for $\beta = 10$. The strength varies with the laminate stacking sequence as well as the LE fiber relative volume fraction. The symbols in Fig. 5.22 correspond to the four types of fiber arrangements (A, B, C and D) in Fig. 5.21. It can also be seen that the hybrid effect is greatest for the case of $V_{LE} = 0.5$.

The probabilistic analysis of Fukunaga, Chou and Fukuda (1989) has led to the following conclusions: (1) The hybrid composite

Fig. 5.22. The median strength vs. relative fiber volume fraction. (After Fukunaga, Chou and Fukuda 1989.)

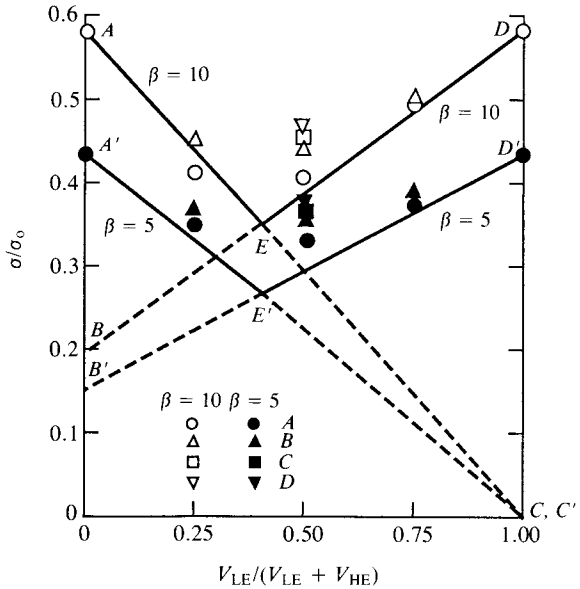

ultimate strength is greater for larger values of shape parameters, whereas the hybrid effect is greater for smaller values of shape parameters. (2) The hybrid effect on the probabilistic ultimate failure strength is most pronounced for $V_{LE} = 0.5$. (3) Both the magnitude and scatter of strengths vary with the length of hybrid composites. (4) The strength is also affected by the lamina stacking sequences because of the difference in stress redistributions resulting from laminar fracture. For a given relative fiber volume fraction, laminates with the LE layers uniformly dispersed among the HE layers are stronger than the laminates with the LE layers clustering together.

5.5 Softening strips

The idea of using softening strips in laminated composites has been developed for the purpose of modifying the local stress state and thus enhancing the load-carrying capability of composite structures. The process of introducing a softening strip involves replacing the low elongation plies with high elongation layers in selected regions, thus forming an interlaminated hybrid composite. Sites of stress concentrations in composites are particularly desirable for the use of softening strips. This concept is demonstrated below for notched laminates.

Sun and Luo (1985) have used three composites for fabrication of the hybrid specimens, i.e. AS4/3501 carbon/epoxy by Hercules, S2/CE9000-9 glass/epoxy by the Ferro Corp., and Scotchply 1002 glass/epoxy by the 3M Co. The base-line carbon/epoxy laminates have the lay-up of $[\pm 45°/0°/0°/0°/\mp 45°]$ and $[\pm 45°/0°]_s$. Each laminate contains a circular hole at the center. To create the softening strips, two plies of S2/CE9000-9 glass/epoxy are used to replace the three 0° carbon/epoxy plies in the $[\pm 45°/0°/0°/0°/\mp 45°]$ laminate, and one ply of Scotchply glass/epoxy is used to replace the two 0° carbon/epoxy layers in the $[\pm 45°/0°]_s$ laminate. Each strip is placed along the axial direction in the center of the laminate. The width of the softening strip is about twice of the hole diameter.

Table 5.4 summarizes the average failure load of all-carbon and hybrid composites. For both laminate systems, there is a significant increase in failure load (22–8%) in the notched hybrid system over the corresponding all-carbon system. However, the unnotched hybrid system shows lower strength than the corresponding all-carbon system as expected. The enhancement in failure load is realized only in the notched specimens. This can be understood from a stress analysis of the hybrid and non-hybrid laminates.

Figure 5.23 presents the results of finite element analysis of the normal stress along the transverse cross-section through the center of the circular hole. The distance in Fig. 5.23 is measured from the edge of the hole. There is a drastic reduction of the stress concentration in the hybridized region due to the presence of the low modulus material. This is believed to be the reason for the higher ultimate strength of the hybrid composite. The stress level outside of the softening strip is elevated.

Table 5.4. *Average maximum load. After Sun and Luo (1985).*

	$[\pm 45°/0°/0°/0°/\mp 45°]$			$[\pm 45°/0°]_s$		
	all-carbon (kN)	hybrid (kN)	Δ (%)*	all-carbon (kN)	hybrid (kN)	Δ (%)*
unnotched	51.6	41.0	−20.5	30.2	21.4	−29.2
notched	27.3	35.0	28.3	15.6	19.1	22.0
Δ (%)†	−47.0	−14.5		−48.2	−10.9	

* Δ(%) = hybrid maximum load/carbon maximum load −1
† Δ(%) = notched maximum load/unnotched maximum load −1

Fig. 5.23. Finite element analysis of axial normal stress distribution along the transverse section in the notched laminate of $[\pm 45°/0°/0°/0°/\mp 45°]$ through the center of the circular hole. (After Sun and Luo 1985.)

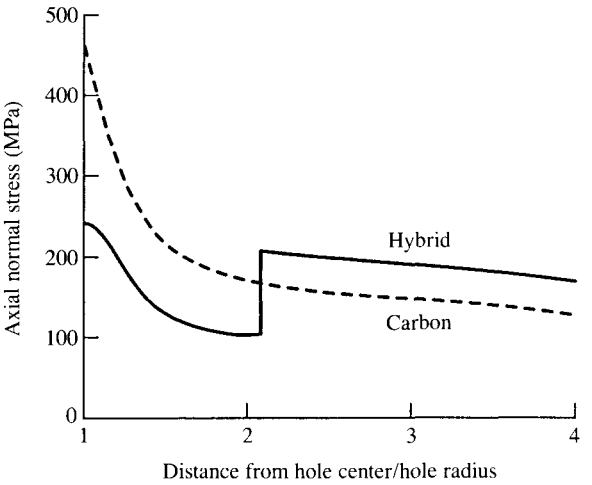

The combination of low elongation and high elongation materials in interlaminated hybrid composites also offers improved fatigue and crack growth properties. A typical example of this kind is the aramid aluminum laminate (also known as ARALL) originated in the Netherlands. (See, for instance, Marissen 1984; Marissen, Trautmann, Foth and Nowack 1984; Mueller, Prohaska and Davis 1985; Vogelesang and Gunnink 1986; Bucci, Mueller, Schultz and Prohaska 1987; Kenaga, Doyle and Sun 1987; Chen and Sun 1989.) ARALL can be considered as a hybrid of aramid fiber laminae sandwiched in between sheets of high strength aluminum alloy. The hybrid composite is 15% less dense than the monolithic aluminum alloy and shows a 100–1000 fold improvement in fatigue life. The tensile properties of the hybrid are reported to be 15–30% better. Thus, ARALL is desirable for fatigue dominated sheet applications such as in lower wing skins, fuselages and tail skins of aircraft.

Other examples of combinations of high elongation and low elongation sheets of materials can be found in the use of adhesive layers in controlling free edge delamination and impact damage. (See, for instance, Chan, Rogers and Aker 1976; Sun and Norman 1988; Sun and Rechak 1988.)

5.6 Mechanical properties

This section discusses briefly the fracture, impact and fatigue characteristics of hybrid composites. In the case of interlaminated hybrid composites the failure mode is the fracture of the low elongation plies transverse to the loading axis. It has been observed in carbon/glass hybrids that the main transverse fracture is typically of cruciform shape and debonding occurs between the carbon and glass plies outwards from the line where the transverse crack intersects the carbon–glass interface. Ultimately most of the hybrid becomes debonded and the strength and stiffness approach those of the glass plies alone as shown in Fig. 5.10 (Bader and Manders 1978; Pitkethly and Bader 1987).

It is important to note that the initial fracture in the carbon plies does not propagate across the glass plies and load can be progressively diffused back into the carbon plies away from the fracture plane (Section 5.3.2). These processes of multiple cracking in the low elongation phase and the associated debonding have a significant effect on the total work of fracture in hybrid composites. The extension of debonding decreases as the absolute thickness of the carbon layers and volume content of carbon fiber decrease. It also has been suggested that debonding could be inhibited if the thickness of the carbon layers is made sufficiently thin.

The subject of work of fracture has received some attention (McColl and Morley 1977; Kirk, Munro and Beaumont 1978). It has been pointed out that fracture mechanisms at the microscopic level in binary fiber composites can be combined to give different kinds of macroscopic fracture behavior in hybrid composites. Therefore the fracture of the carbon/glass hybrid system, for instance, is expected to show characteristics of the individual composite systems.

The impact resistance of composite materials can be modified through a broad range of methods. Jang *et al.* (1989) have reviewed the major techniques including the control of fiber/matrix interfacial adhesion, matrix modifications, lamination design, through-the-thickness reinforcements, fiber hybridization, and utilization of high-strain fibers. Among these approaches, hybrids offer the benefit of improving the impact resistance of composites based upon high modulus fibers.

The total strain-energy of a composite at its ultimate tensile strength is inversely proportional to the fiber tensile modulus. Thus, high modulus fibers are not desirable for impact resistance from the viewpoint of energy absorption. The same is true when the work of fracture or toughness is considered. Aveston and Kelly (1980) have assessed the effectiveness of hybrid composites in energy absorption. Their analysis is recapitulated in the following. Consider the idealized stress–strain curve of Fig. 5.10, and compare the total energy per unit volume absorbed in a hybrid up to its ultimate tensile strength with the sum of energies of its components. By assuming a mean crack spacing of $1.5x$ (for crack spacing between x and $2x$), the strain at the limit of multiple cracking is $\varepsilon_{\mathrm{Lu}}(1 + (\frac{5}{8})\alpha)$ where α is given in Eq. (5.42). The ultimate failure strain of the hybrid is $\varepsilon_{\mathrm{Hu}} - (\frac{3}{8})\alpha\varepsilon_{\mathrm{Lu}}$, where $\varepsilon_{\mathrm{Lu}}$ and $\varepsilon_{\mathrm{Hu}}$ are the ultimate strains of the LE and HE components, respectively.

Based upon these strain values, the area under the stress–strain curve $OABC$ of the hybrid composite is

$$U_1 = \tfrac{1}{8}\alpha E_c \varepsilon_{\mathrm{Lu}}^2 + \tfrac{1}{2}\varepsilon_{\mathrm{Hu}}^2 E_{\mathrm{HE}} V_{\mathrm{HE}} \tag{5.74}$$

When the HE and LE components are completely debonded, the stress–strain curve follows the path $OAEF$. Then the energy absorbed at ultimate failure is

$$U_2 = \tfrac{1}{2}E_c \varepsilon_{\mathrm{Lu}}^2 + \tfrac{1}{2}E_{\mathrm{HE}} V_{\mathrm{HE}} \varepsilon_{\mathrm{Hu}}^2 - \tfrac{1}{2}E_{\mathrm{HE}} V_{\mathrm{HE}} \varepsilon_{\mathrm{Lu}}^2 \tag{5.75}$$

Aveston and Kelly have concluded that for $U_1 > U_2$, α should be greater than three. For the combination of glass and carbon fiber

composites, this can be achieved with a carbon fiber volume fraction of over 30%. Furthermore, the condition of multiple cracking (Eq. (5.41)) requires that $\alpha > 7.1$ for $\varepsilon_{Hu} = 2.3\%$ and $\varepsilon_{Lu} = 0.28\%$. This implies $V_{LE} = 48\%$. Thus, toughening through fiber hybridization and multiple cracking can be accomplished in carbon/glass composites with carbon fiber volume fraction between 30% and 48%.

Experimental studies of the impact behavior of hybrid composites can be found in the work of Chamis, Hanson and Serafini (1972), Beaumont, Riewald and Zweben (1974), Adams (1975), Adams and Miller (1975, 1976), Dorey, Sidey and Hutchings (1978); Adams and Zimmerman (1986); and Jang *et al.* (1989). Several test methods have been employed to measure the impact resistance of composite materials. The Charpy impact test and Izod impact test have been performed mainly on unidirectional composites, whereas the drop-weight impact test is usually used for laminated composites. Other tests such as longitudinal impact, transverse impact and pure shear impact tests on unidirectional fiber composites have also been considered.

Both notched and unnotched specimens have been used in Charpy tests. Instrumented Charpy impact tests can be used to determine the maximum load on the specimen, as well as to differentiate between the energy required to initiate damage and the energy absorbed during damage propagation. The relative sizes of the two regions for failure initiation and propagation under the load–time curve provide a qualitative measurement of the ductility of a composite under impact loading. Two materials with the same total Charpy energy may have quite different proportions of the component energies and, thus, distinct mechanisms of failure (Beaumont, Riewald and Zweben 1974). Most composite materials, especially laminated systems, can dissipate a considerable amount of energy in the fracture propagation phase even though the initial fracture may be of a brittle cleavage mode (Adams and Miller 1975). Interlaminated hybrid composites have been found to increase delamination under impact loading. Jang *et al.* (1989) have reported that the impact energies of the interlaminated hybrids generally show a negative hybrid effect, i.e. slightly lower energy dissipation than that predicted by the rule-of-mixtures.

As to the fatigue behavior of hybrids, Phillips (1976) has reported significant improvements in fatigue resistance of glass composites by hybridization with carbon fibers. At the stress level of 300 MPa or about 50% of ultimate, the fatigue life of the three-to-one volume fraction of glass/carbon hybrid is improved by about 100 fold over

the all-glass control. This probably arises from the increased stiffness and, hence, the decreased strain for a given stress.

Figure 5.24 shows the stress vs. log life curves for unidirectional carbon/Kevlar hybrids tested in repeated tension (minimum stress/maximum stress = 0.1) reported by Fernando *et al.* (1988). The stresses in Fig. 5.24 are peak stresses. The σ_{max}/log N curves show a uniform variation from the linear form of the curve for plain carbon/epoxy towards the pronounced step-function shape of the curve for the plain Kevlar-49/epoxy composite. Adam et al. (1989) have examined a series of carbon/Kevlar-49/epoxy unidirectional hybrid composites; the fatigue behavior has been established as a function of composition and the ratio of the minimum to maximum stress in cyclic tension and tension/compression. This enables them to represent all data in a single two-parameter fatigue curve.

Other mechanical property data can be found in the literature for the non-linear tensile stress–strain relation (Takahashi and Chou 1987), compressive behavior (Chou, Steward and Bader 1979; Chou and Kelly 1980b; Gruber, Overbeeke and Chou 1982; Kretsis 1987; Yau and Chou 1989), flexural behavior (Fischer and Marom 1987; Marom and Chen 1987) and shear property (Kretsis 1987).

Fig. 5.24. Stress/log life (σ_{max}/log N) curves for the family of unidirectional carbon/Kevlar hybrids tested in repeated tension (minimum stress/maximum stress = 0.1). (After Fernando *et al.* 1988.) σ_{max} is the peak stress. The percentages indicate relative fiber volume fractions of carbon and Kevlar.

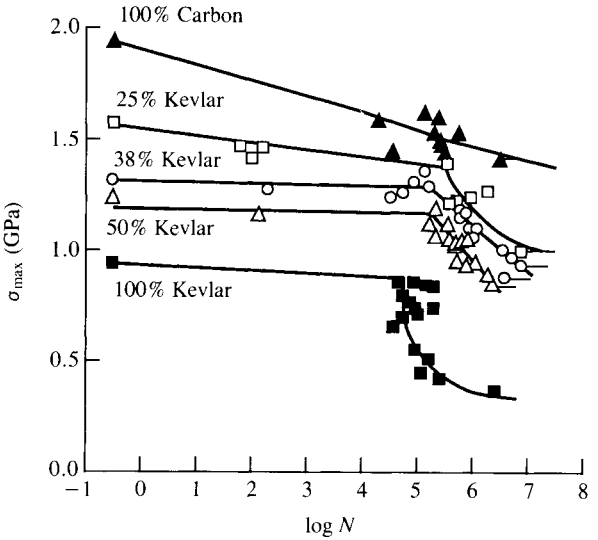

5.7 Property optimization analysis

5.7.1 *Constitutive relations*

A method is presented in this section to determine the concentration of components which can simultaneously optimize certain mechanical, thermal and electrical properties of a hybrid composite. This analysis, developed by McCullough and Peterson (1977) is essential in the pursuit of balanced material properties of a multi-component system.

The basis of this optimization analysis is the assumption that the constitutive relations for several major properties can be cast into simple linear form. Although the hybrids under consideration are restricted to unidirectional composites, the general format of this treatment is applicable to structural elements with more complex fiber arrangements. The constitutive equations for estimating the longitudinal properties of ternary composites are summarized below. Here, the volume fractions of the components are denoted by V, and the weight fraction by w. The subscripts 1, 2 and 3 refer to the components of the ternary system.

Mechanical properties

$$\begin{aligned} &\text{modulus} && E = V_1E_1 + V_2E_2 + V_3E_3 \\ &\text{strength} && \sigma = (V_1E_1 + V_2E_2 + V_3E_3)\varepsilon^* \\ &\text{Poisson's ratio} && \nu = V_1\nu_1 + V_2\nu_2 + V_3\nu_3 \end{aligned} \tag{5.76}$$

Thermal properties

$$\begin{aligned} &\text{coefficient of expansion} && \alpha = [V_1E_1\alpha_1 + V_2E_2\alpha_2 + V_3E_3\alpha_3]/[V_1E_1 + V_2E_2 + V_3E_3] \\ &\text{thermal conductivity} && K = V_1K_1 + V_2K_2 + V_3K_3 \end{aligned} \tag{5.77}$$

Electrical property

$$\begin{aligned} &\text{resistivity} && \frac{1}{\rho} = \frac{V_1}{\rho_1} + \frac{V_2}{\rho_2} + \frac{V_3}{\rho_3} \\ &\textit{Weight density} && d = V_1d_1 + V_2d_2 + V_3d_3 \end{aligned} \tag{5.78}$$

Cost

$$\text{cost/weight} \qquad C = C_1w_1 + C_2w_2 + C_3w_3 \tag{5.79}$$

In the strength expression it is assumed that $\varepsilon^* = \min(\varepsilon_1, \varepsilon_2, \varepsilon_3)$ and failure occurs when the composite strain reaches the lowest failure strain of the three components. Clearly, this assumption

underestimates the longitudinal strength. In the cases of coefficient of expansion and resistivity, E, α and ρ are treated as property variables. Also, w_i is the weight fraction of the ith component.

It is often useful to examine the performance of a composite in terms of certain 'specific' properties (i.e. the property per unit weight). A specific property $\bar{P}$ can be related to the property P and its weight density d as

$$\begin{aligned}\bar{P} &= \left(\sum_{i=1}^{3} P_i V_i\right) \Big/ \left(\sum_{j=1}^{3} d_j V_j\right) \\ &= \sum_{i=1}^{3} \left[(d_i V_i) \Big/ \left(\sum_{j=1}^{3} d_j V_j\right)\right] P_i/d_i \\ &= \sum_{i=1}^{3} \bar{P}_i w_i \end{aligned} \tag{5.80}$$

where w_i is defined by the term in the square brackets. The equations for mechanical, thermal and electrical properties, as well as density, have volume fraction as the composition variable while the specific property equations and the cost equation have weight fraction as the composition variable. Volume fraction and weight fraction are related by

$$w_i = d_i V_i / d \tag{5.81}$$

Both weight fraction and volume fraction can be used as concentration variables in the analysis of performance.

A typical property map for ternary systems can be represented by triangular diagrams as shown in Fig. 5.25. Each side of the equilateral triangle is unity in length and it expresses the volume fraction of a component. The volume fraction of a ternary system is represented by a point inside the triangle. For example, the hybrid composite denoted by point R in the property map contains 35%, 25% and 40% of matrix, fiber 1 and fiber 2, respectively. These concentration readings are obtained by drawing lines from point R parallel to the three sides of the triangle. The volume fractions of binary systems and pure components are represented, respectively, by points located on the sides and the apices of the triangle.

A straight line within the triangle of Fig. 5.25 specifies arbitrarily selected property levels available to the ternary system. Thus, line DE represents the various ways of combining the three components to achieve a specified property level, P, of the composite. Point E, for example, indicates that the combination of 55% volume fraction of matrix, 0% volume fraction of fiber 1 and

45% volume fraction of fiber 2 will result in a composite with property P. This same property level P can be achieved by concentration levels represented by all the other points on line DE. Also shown in Fig. 5.25 is the shaded area defined by the concentration line for 20% of matrix material. This particular volume fraction represents a square array of fibers of equal size. By determining the minimum desirable volume fraction of matrix material, the region in the triangle representing a matrix content below the minimal level can be excluded from further consideration in the optimization process.

Figures 5.26(a) and (b) present the various levels of longitudinal specific modulus and longitudinal specific strength of the hybrid system. The lines of constant properties are constructed from the following property data for the carbon/boron/epoxy system: Young's modulus in GPa (345/410/3.4); tensile strength in GPa (2.1/3.1/0.035); density in 10^3 kg/m^3 (1.66/2.71/1.1); critical strain in % (0.6/0.7/10).

Fig. 5.25. Typical format of a ternary property map. (After McCullough and Peterson 1977.)

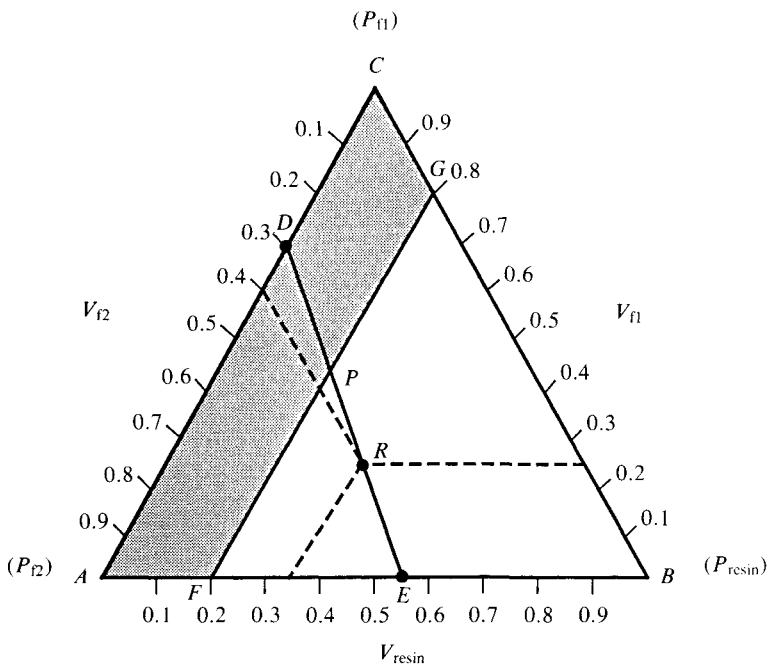

5.7.2 *Graphical illustration of performance optimization*

Figure 5.27 illustrates the property map for two different composite properties P and Q. For clarity only one of the constant property levels of property P is shown. It can be readily demonstrated that a designer can achieve a specified property of the hybrid by simultaneously adjusting the component properties.

Fig. 5.26. Selected property maps for the system carbon/boron/epoxy. (a) specific modulus. (b) Specific strength. (After McCullough and Peterson 1977.)

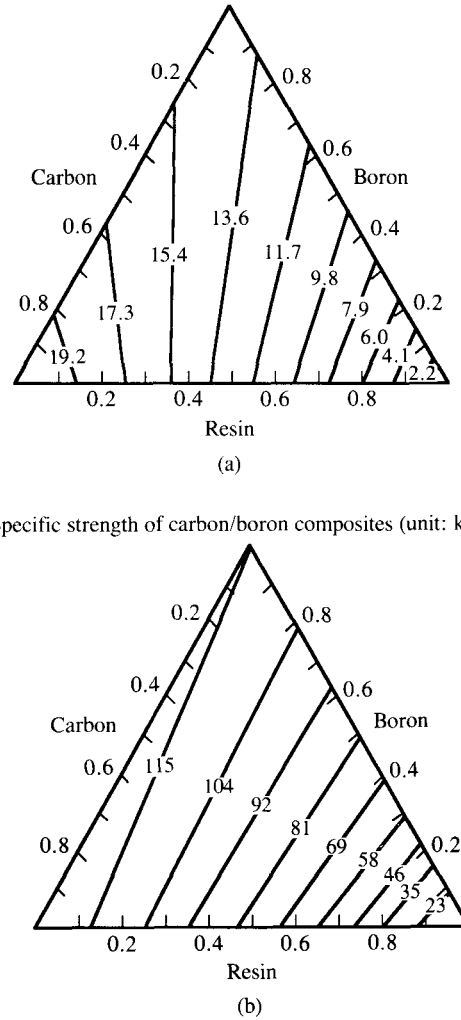

Any combination of fiber and resin that falls on line P will yield a composite with property P. Similarly, a line denoted by Q_j represents a specified level of property Q achieved by combinations of fiber and resin properties. Any combination of components that falls simultaneously on lines P and Q_j will yield a hybrid composite with properties P and Q_j. Consequently, the intersection of lines P and Q_j uniquely determines the concentrations of the three components to achieve properties P and Q_j.

Suppose that $Q_1 < \cdots < Q_i < \cdots < Q_7$. If a hybrid composite is desired such that for a specified property P (e.g. modulus), the property Q (e.g. strength) is a maximum, then the intersection of P and Q_7 should give the proper combination of concentrations of the components.

It often occurs in the optimization of hybrid composite design that, instead of a specified property, a level of performance is required. For instance, a property level P or greater (or P or less for properties such as density and cost) may be required. Figure 5.28 illustrates superimposed maps for properties P and Q. The requirements are

$$\begin{aligned} P &> P^* \\ Q &> Q^* \end{aligned} \tag{5.82}$$

and

$$V_{\text{matrix}} > V_0$$

Fig. 5.27. Superimposed property maps for properties 'P' and 'Q'. (After McCullough and Peterson 1977.)

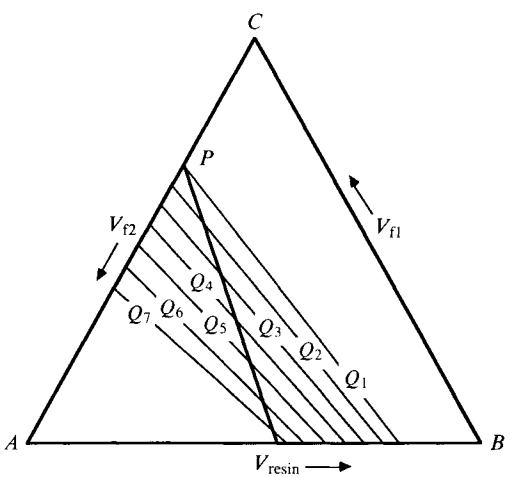

Fig. 5.28. Superimposed property maps illustrating bounding ranges on performance requirements. (After McCullough and Peterson 1977.)

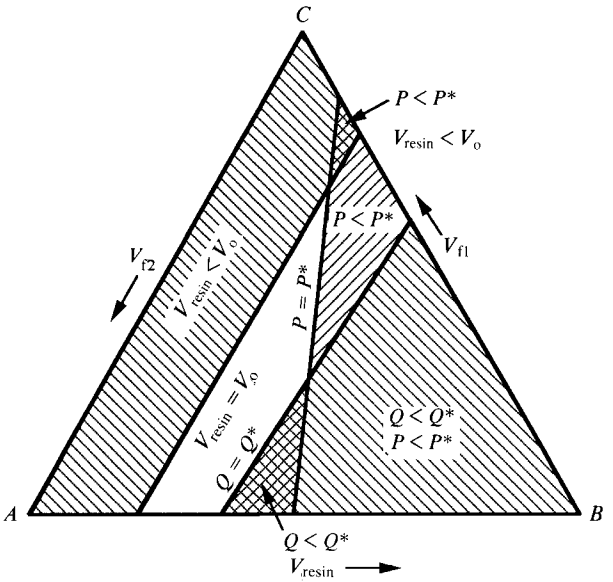

The shaded regions in Fig. 5.28 represent the concentration ranges which fail to meet any one or all of the above requirements. Naturally, the concentration ranges in the unshaded area of the figure will meet or exceed the specified requirements. The optimization of hybrid composite performance can thus be carried out based upon the basic information given in the property maps of the type shown in Fig. 5.26.

This schematic treatment illustrates the basic notions for a performance optimization of multicomponent systems. When the number of components exceeds three, the graphical method is no longer applicable. McCullough and Peterson (1977) have developed algebraic relationships of the properties of multicomponent systems and the optimization procedure has been structured in the form of a classical linear programming problem.